TECHNICAL MEMORANDUM

ANL-CT-81-34

Distribution Category:
Light Water Reactor Technology
(UC-78)

ARGONNE NATIONAL LABORATORY
9700 South Cass Avenue
Argonne, Illinois 60439

A THREE-DIMENSIONAL SIMULATION OF DIVERSION CROSS-FLOW BETWEEN TWO PARALLEL CHANNELS CONNECTED BY A NARROW LATERAL SLOT USING THE COMMIX-1A COMPUTER PROGRAM

by

H. P. Fohs*

Northwestern University
Evanston, Illinois

and

R. W. Lyczkowski and W. T. Sha

Components Technology Division

October 1981

*Participant in the Summer 1981 Student Research Participation Program, which is coordinated by the Division of Educational Programs, ANL.

Table of Contents

ABSTRACT:

This report demonstrates the predictive capabilities of the COMMIX-1A computer program by simulating a fundamental experiment which determined diversion cross-flow and pressure drops between and along two parallel square channels connected by a narrow lateral slot. COMMIX-1A predicted correct trends and fairly accurate flow quantities with minimum empirical input.

INTRODUCTION AND BACKGROUND:

The purpose of this project is to verify and demonstrate the predictive capabilities of the COMMIX-1A computer program. This is accomplished by comparing the experimental results of Tapucu and Merilo's experiments [1,2] with results from the computer simulation of their experiment.

The Tapucu and Merilo experiments measured the diversion cross-flow between two parallel square channels connected by a long, narrow lateral slot. The pressure drop across the slot is correlated to the cross-flow velocity by a dimensionless friction coefficient, K. The experiment is performed at several different inlet velocities and slot dimensions. The results show the variation of this friction coefficient with geometry and velocity ratios. Figure 1 shows the geometric configuration of the experimental apparatus.

COMMIX-1A was developed to analyze three-dimensional, transient, single-phase, thermal-hydraulic flow in reactor components. The governing equations for conservation of mass, momentum, and energy are solved as a boundary-value problem in space and as an initial-value problem in time. The numerical solution technique solves the governing equations using a staggered mesh finite differenced formulation. Three-dimensional Cartesian geometry was used for the geometric configuration shown in Fig. 1. In the staggered mesh system, all the fluid properties, except velocity, are evaluated at the cell center. The velocity components are evaluated at the cell edges [3].

The major trade-off in this flow simulation is the accuracy of the flow quantities versus the quantity of computational cells. The accuracy of the flow simulation increases with the number of cells, but the cost of making the simulation run also increases.

PROCEDURE:

The geometry of the experimental apparatus is input into the computer program by specifying the maximum number of cells in each direction, the cell length associated with each of the three directional indices, and the cells having boundary surfaces. The first computer simulation run, TAPC01, was limited to a total number of 1200 cells. This limitation led to a coarse computational mesh as shown in Figure 2, which also shows representative velocity vector plots. The smaller dimensioned cells were placed in areas where high pressure gradients causing high cross-flows were expected. Only one-half of the total flow field is calculated since there is a y-plane of symmetry through the slot center. The choice of the computational mesh of the second simulation run, TAPC02, Figure 3, is largely based on the results of the first run and was also limited to a reasonable total number of cells. More cells were added in the z-direction to reduce the large pressure jumps calculated in TAPC01 and to improve the pressure drop curve resolution. To improve the accuracy of the diversion cross-flow mass transfer, the number of cells across the slot gap clearance, y-direction dimension, was increased from 2 to 4 cells. The total number of cells for the TAPC02 run is 2312.

The z-direction length of the flow inlet cells was increased to develop a more realistic non-uniform velocity distribution in the donor channel. The z-direction length of the flow outlet cells was increased to match the experimental pressure drop at the outlet.

The boundary condition used in the simulation for the donor channel inlet surface is a uniform specified inlet velocity of 1.559 m/s. This is the area averaged velocity determined by dividing the reported volumetric flow rate of 0.905 m^3/hr by the channel cross-sectional area of 161.3mm^2. The specified velocity for the recipient channel inlet surface remained zero for all computer runs [3].

Both the donor and recipient channel outlets have a common continuative mass flow outlet boundary condition [3]. This condition closely approximates equalized pressure at the outlet cell centers of both channels. By positioning the outlet cell centers further downstream, the experimental outlet pressure drop boundary condition was met.

The state of water at 20° Celsius and standard atmospheric pressure was used to obtain the values of density (997.2 kg/m^3) and laminar viscosity (0.001 Pa·s). Isothermal conditions were assumed.

In order to simulate turbulent flow, COMMIX-1A adds an effective turbulent viscosity to the laminar viscosity and then uses their sum in the evaluation of the viscous shear stress terms at every mesh point in the flow field. The effective turbulent viscosity was estimated from Eq. B.1 in Ref. 3 to be 0.005 Pa·s. The donor channel inlet flow properties and hydraulic diameter were used in this evaluation.

For the cross-flow in the slot, the local Reynolds number is in the laminar region. Therefore, the turbulent viscosity was set to zero for the third simulation run, TAPCO3, to determine the effect of this turbulent viscosity.

In the experiment, the pressures were measured on the transverse centerline of the slot at the outer channel walls in regular intervals along the channel height. These points correspond to the two x-edges of the y-plane of symmetry used as a surface boundary in this flow model. Therefore, the adjacent corner cell center pressures at each K level are used to simulate the experimental measurements. In index notation, the donor channel pressure at any K level is associated with the I=17, J=8 cells for the TAPCO2 and TAPCO 3 runs.

The recipient channel pressures are associated with the I=1, J=8 cells. These computed pressures were used to construct the axial pressure curves and to calculate the differential pressure across the slot by subtracting the recipient channel pressure from the donor channel pressure. For comparison purposes, Table 1 in Appendix A lists the differential pressures calculated as above next to differential pressures calculated from the pressure for cells immediately adjacent to the slot inlet and outlet. Almost all the pressure drop occurs in the slot.

The integral cross-flow mass transfer of any axial distance z is defined as the double integral

$$\dot{m}_{cf}\Big|_{z} = - \int_{\substack{\text{slot}\\ \text{start}}}^{z} \int_{\substack{\text{gap}\\ \text{clearance}}} \rho \, v_{xe} \, dy \, dz \qquad (1)$$

where:

$\rho \equiv$ density

$v_{xe} \equiv$ x-component of velocity on the slot exit plane (negative from right to left).

For TAPCO2 and TAPCO3, this integral is approximated by the double summation shown below:

$$\dot{m}_{cf}\Big|_{KH} = -2\rho \sum_{K=5}^{KH} \sum_{J=7}^{8} UL(7,J,K) \cdot DY(J) \cdot DZ(K) \qquad (2)$$

where:

KH $\equiv$ K level associated with desired height

UL(I,J,K) $\equiv$ x-component velocity at mesh location I,J,K

DY(J) $\equiv$ y-direction cell length

DZ(K) $\equiv$ z-direction cell length

For TAPCO2, the area averaged transverse velocity exiting the slot is calculatd as shown below:

$$\overline{UL}_{E} = - \sum_{J=7}^{8} UL(7,J,K) \cdot DY(J) \cdot DZ(K) \quad A_{SLOT\ C.S.} \qquad (3)$$

where:

$$A_{SLOT\ C.S.} \equiv [DY(7) + DY(8)] \cdot DZ(K)$$

The tables in Appendix A list the data and results associated with these calculations. For TAPCO2, the double summation shown below is used to calculate the area averaged donor channel velocity:

$$\overline{WL_D} = \sum_{I=11}^{17} \sum_{J=1}^{8} WL(I,J,K) \cdot DX(I) \cdot DY(J) \quad A_{C.S.} \qquad (4)$$

where:

$WL(I,J,K) \equiv$ z-component velocity at mesh location I,J,K

$DX(I) \equiv$ x-direction cell length

$A_{C.S.} \equiv$ cross-sectional area of channel

The results from the above calculations are then used in the following equation to calculate the transverse resistance coefficient:

$$K_R = \frac{\Delta P}{\frac{1}{2} \rho \left(\overline{uL_E}\right)^2} \qquad (5)$$

RESULTS:

The major results are presented graphically with details given in Appendix A.

Figure 4 compares the computed pressure drops minus the gravity head across the slot *vs* channel height for all three runs with the experimental results. The differential pressure curves computed from TAPC01 and TAPCO2, shown in Figure 4, follow the trend of the experimental data and graphically illustrate the effect of decreased mesh size on the accuracy. Just as significant is the departure of the TAPCO3 differential pressure curve from the data. Since the only difference between the TAPCO2 run and the TAPCO3 run is the removal of the effective turbulent viscosity, clearly its value has an effect on the simulation.

Figure 5 compares the cross-flow mass transfer for all three runs and the experiment. Figure 6 compares the variation of absolute pressure minus gravity head versus channel height for the last two runs and the experiment.

The comparison of axial pressure drops made on Figure 6 has several interesting implications. One is that since the TAPCO2 and TAPCO3 runs both differ significantly from the experimental data, neither is an accurate simulation of the experiment. However, as Figures 4 and 6 show, the agreement with the experimental pressure drop across the slot and the cross flow mass transfer is fairly good for the TAPCO2 run. With a turbulent viscosity of five times the laminar viscosity (TAPCO2 run) the pressure in the donor channel decreases, then levels off before decreasing again. With zero turbulent viscosity (TAPCO3), the pressure drop goes through a minimum. This is the same trend as the data, but the TAPCO3 simulation is highly inaccurate. The computed trends for the axial pressure drop in the recipient channel are basically the same as the data. These trends imply that a constant effective turbulent viscosity used globally can be adjusted to give better agreement with the data for the same mesh size used for TAPCO2 and TAPCO3.

Figure 5 again shows that the TAPCO2 run calculated the most accurate cross-flow of the three runs. One implication from the comparison of these curves is that the reduction of turbulent viscosity, which may give better pressure drop agreement, will not increase the accuracy of the cross-flow calculated. Another implication from the comparison of the TAPCO1 and TAPCO2 curves is that reduced mesh size does lead to more accurate cross flow calculation, both in trend shape and quantity.

Figures 7, 8, and 9 compare pressure drops, cross-flow mass transfer, and pressure variations between only TAPCO2 and the experiment. Figure 10 compares the computed average axial velocity in the donor channel with the data. Figure 11 compares the calculated transverse resistance coefficient versus velocity ratio between TAPCO2 and the experiment.

Figure 11 shows that the transverse resistance coefficient curve of the TAPCO2 run trends very well and has good agreement with the experiment in the low velocity ratio region with decreasing accuracy as the velocity ratio increases. The TAPCO2 data point with the largest deviation from the experimental curve is calculated from the flow properties of the first cell level above the slot start. In this region, the velocity and pressure jumps are large due to the appearance of the slot Further decreased mesh size should improve the accuracy of the calculations in this region.

Figures 12 through 31 illustrate the computed cell center velocity vectors of the TAPCO2 run for various cross-sectional planes of interest. A "J" plane is a constant y-coordinate plane cutting through the cell centers associated with that particular J index number. Similarly, a "K" plane is a constant z-coordinate plane associated with that K index number.

Figures 32 through 42 similarly illustrate the velocity vectors of the TAPC03 run.

Several significant observations can be made from the velocity vector plots, Figures 12 thorough 42. One observation is the expected recirculation patterns seen in the "K" plane figures, which vary in strength from level to level. TAPC01 velocity vector plots had similar patterns on a coarser mesh grid. The large jump in the x-component velocity at the corner of the donor channel and the slot start is clearly seen in Figures 14, 15, and 18. Again similar observations were made from the TAPC01 and TAPC03 plots. One interesting comparison between the TAPC02 and TAPC03 "J" plane plots, Figures 14, 15, 32, and 33, is the more rapid decrease of the TAPC02 velocity magnitudes in the slot region. Another interesting comparison between the TAPC02 and TAPC03 "K" plane plots is the less rapid change of the TAPC03 recirculation strength from level to level. The implication from both these comparisons is that the removal of turbulent viscosity results in more overall recirculation and less pressure drop through the slot region.

The velocity vector plots also show that this problem can be divided into three characteristic flow regions. The first is a region of high turbulent parallel flow in the donor channel, the second is a region of low, less turbulent parallel flow through a narrow slot, and the third is a region of medium turbulent recirculating flow in the recipient channel which again becomes mostly parallel flow after the slot end.

CONCLUSIONS:

The COMMIX-1A Computer Code has been found to predict correct and accurate trends for pressure differences and mass transfer between channels using a constant value of effective turbulent viscosity. The predicted pressure drops in the axial direction for each channel have the correct trends but are very sensitive to the variation in effective turbulent viscosity. It appears that an effective turbulent viscosity can be found which yields good agreement with the pressure drop data but the computed mass transfer rate is consistently below the data with a maximum deviation of 20-25%. Private communications from Merilo and Tapucu [4] indicate that the COBRA code could not calculate this problem due to high cross-flows.

Two courses of future investigation are possible. The first is to further reduce the mesh size in the high gradient regions at the slot start. The cost effectiveness of this approach is questionable, however, since the computer running time will increase considerably. The second is to add a more local turbulence model. This may be necessary since the experiment has no imbedded internal structure. In addition the turbulence is considerably higher in the channels than in the slot. Considering the prediction of the correct trends and fairly accurate cross-flow mass transfer, the use of an effective turbulent viscosity appears sufficiently accurate for engineering purposes.

REFERENCES:

1. A. Tapucu, "Studies on Diversion Cross Flow between Two Parallel Channels Communicating by a Lateral Slot. I: Transverse Flow Resistance Coefficient," Nuclear Engineering and Design, Vol. 42 (1977) pp. 297-306.

2. A. Tapucu and M. Merilo, "Studies on Diversion Cross Flow between Two Parallel Channels Communicating by a Lateral Slot. II: Axial Pressure Variations," Nuclear Engineering and Design, Vol. 42 (1977), pp. 307-318.

3. W. T. Sha, H. M. Domanus, R. C. Schmitt, J. J. Oras, and E. I. H. Lin, "COMMIX-1: A Three-Dimensional Transient Single-Phase Component Computer Program for Thermal-Hydraulic Analysis," Prepared by Argonne National Laboratory, Components Technology Division, for the U. S. Nuclear Regulatory Commission, Document, No. NUREG/CR-0785, ANL-77-06 (1978).

4. M. Merilo and A. Tapucu, Private Communications, Aug, 1981.

Figure 1

TAPUCU EXPERIMENTAL APPARATUS

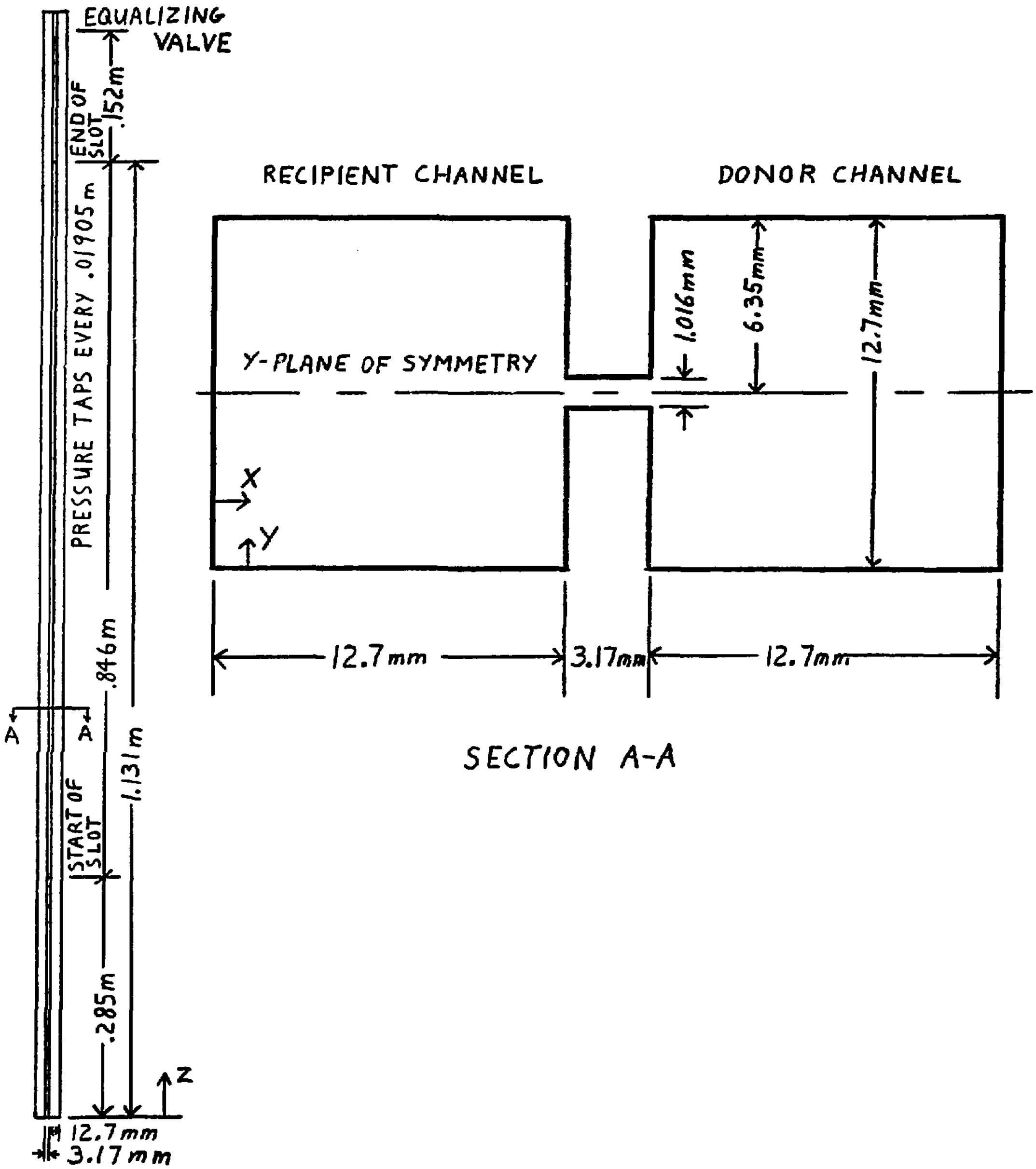

SECTION A-A

Figure 2

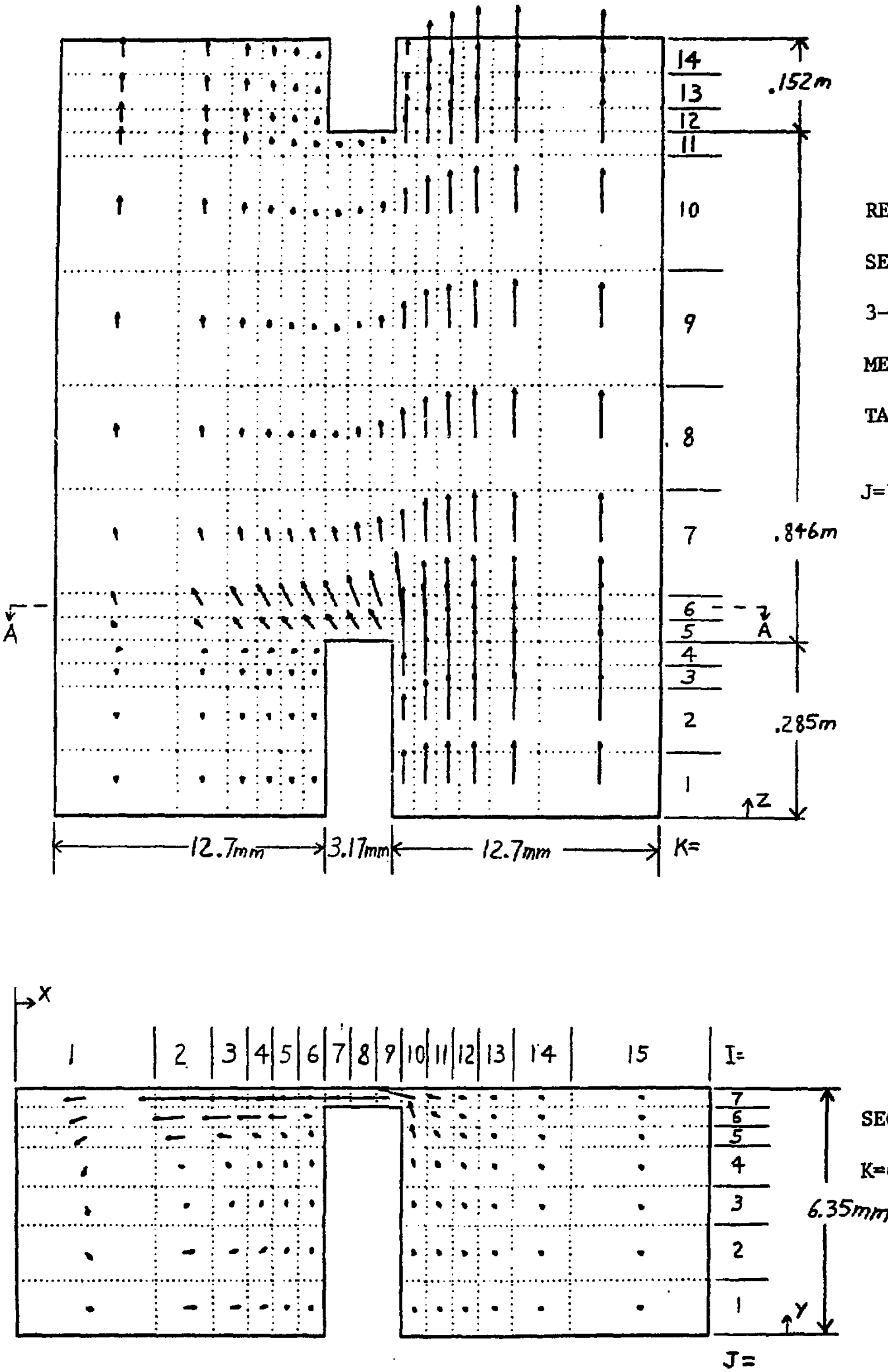

REPRESENTATIVE SECTIONS OF 3-D COMPUTATIONAL MESH FOR TAPC01

J=7 PLANE

SECTION A-A

K=6 PLANE

Figure 3

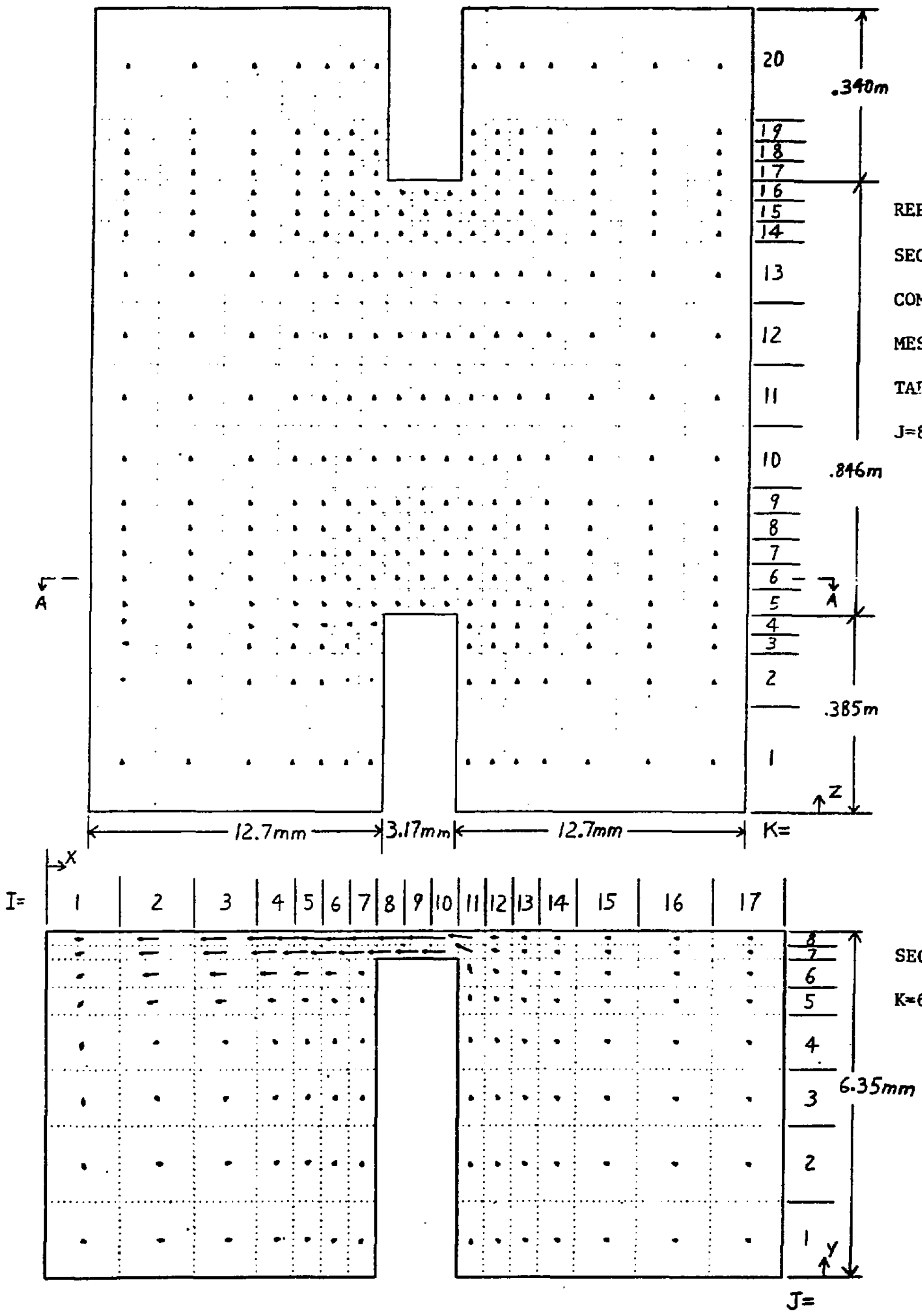

REPRESENTATIVE SECTIONS OF 3-D COMPUTATIONAL MESH FOR TAPCO2 J=8 PLANE

SECTION A-A K=6 PLANE

DIFFERENTIAL PRESSURE ACROSS SLOT VERSUS CHANNEL HEIGHT

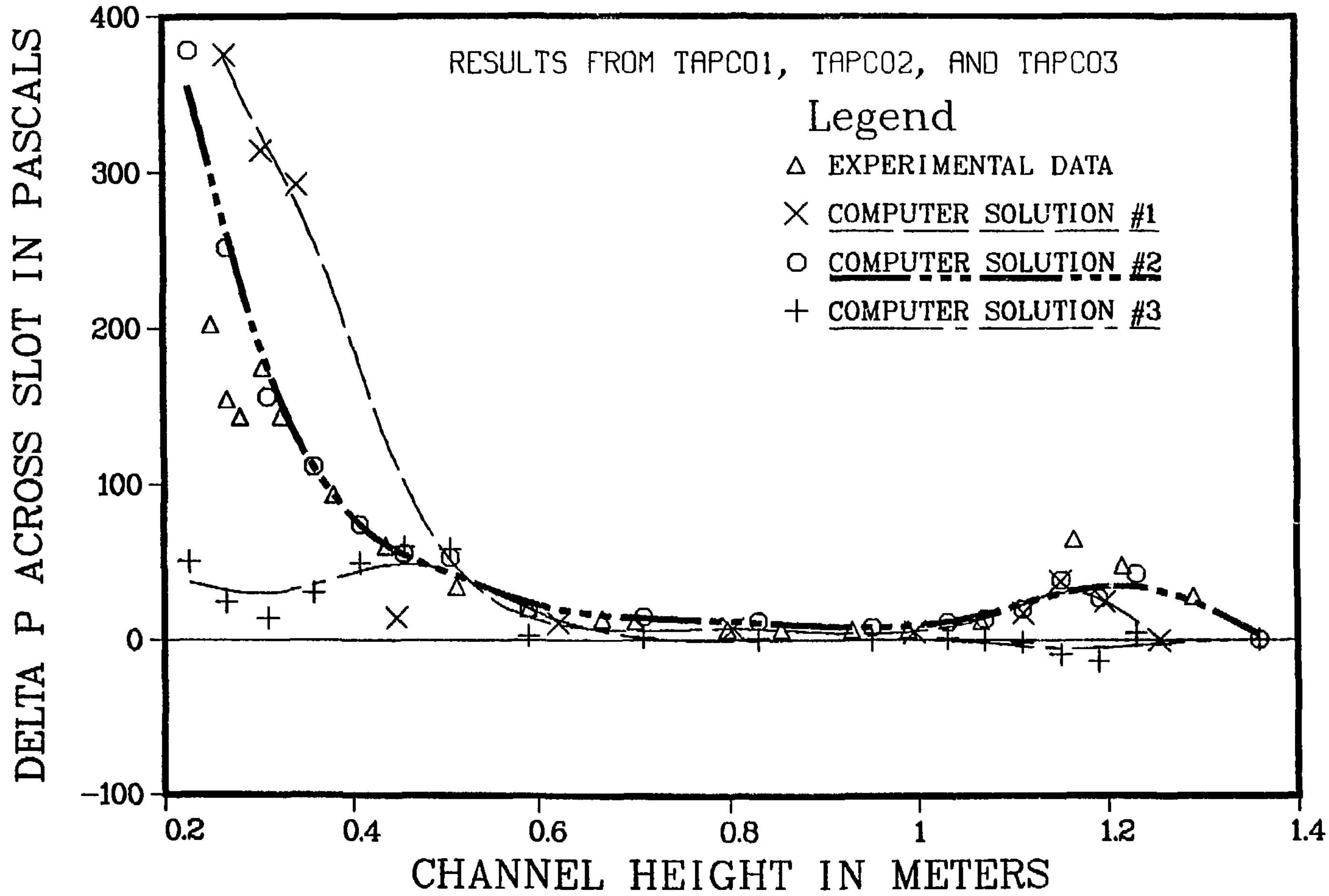

Figure 4

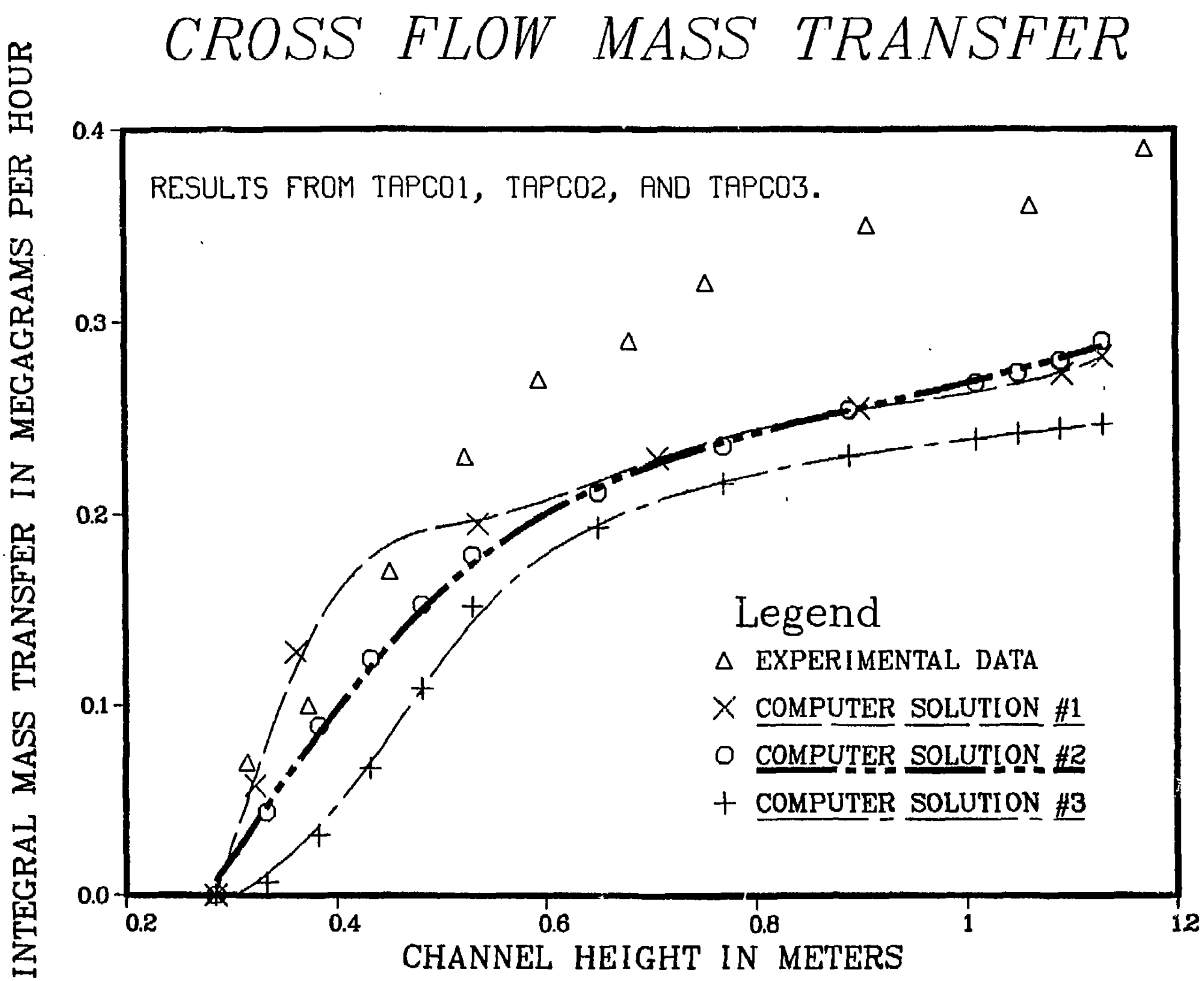
CROSS FLOW MASS TRANSFER
RESULTS FROM TAPC01, TAPC02, AND TAPC03.
INTEGRAL MASS TRANSFER IN MEGAGRAMS PER HOUR
0.4
0.3
0.2
0.1
0.0
0.2
0.4
0.6
0.8
1
12
CHANNEL HEIGHT IN METERS
Legend
EXPERIMENTAL DATA
COMPUTER SOLUTION #1
COMPUTER SOLUTION #2
COMPUTER SOLUTION #3

Figure 5

AXIAL PRESSURE VERSUS CHANNEL HEIGHT

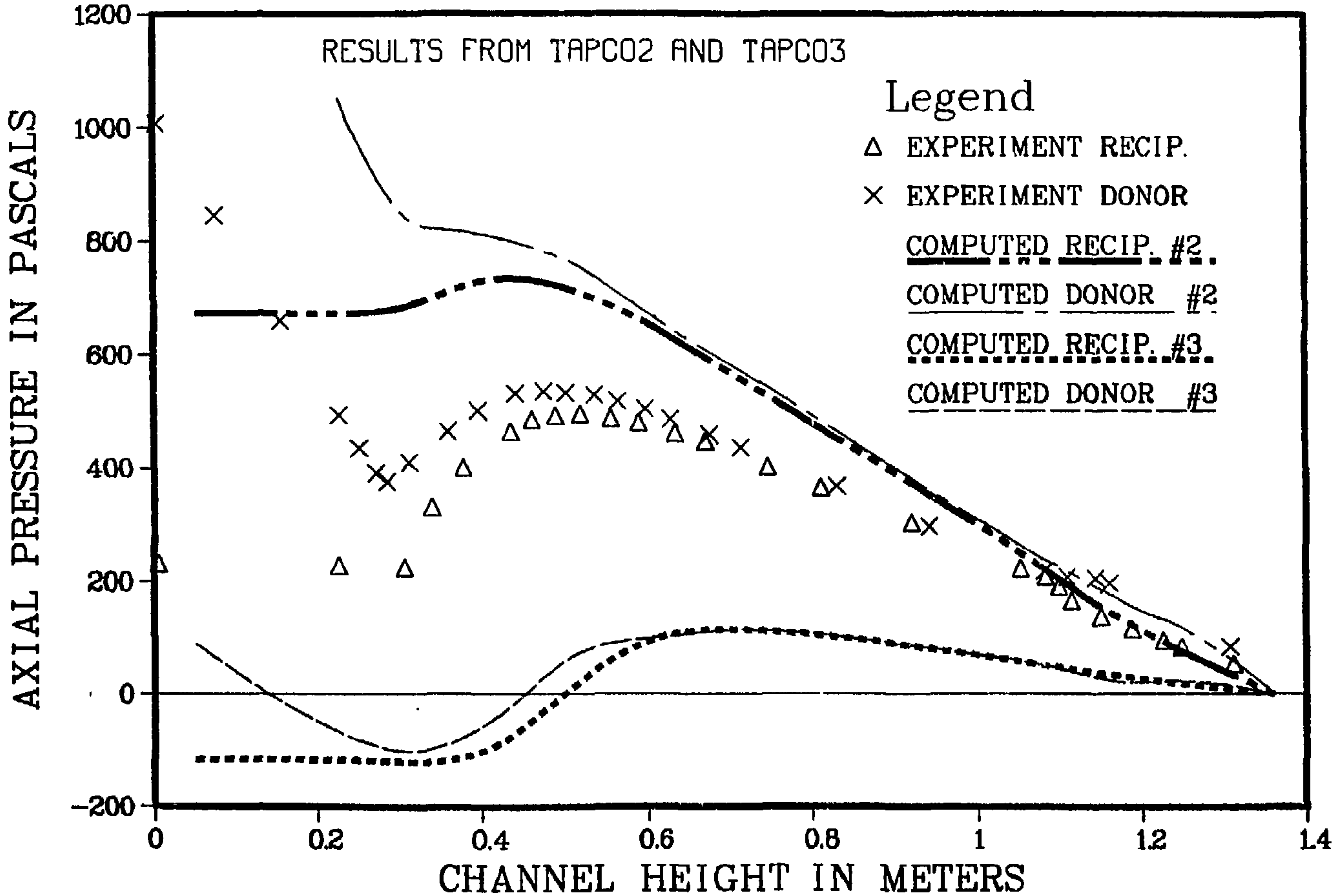

Figure 6

DIFFERENTIAL PRESSURE ACROSS SLOT VERSUS CHANNEL HEIGHT

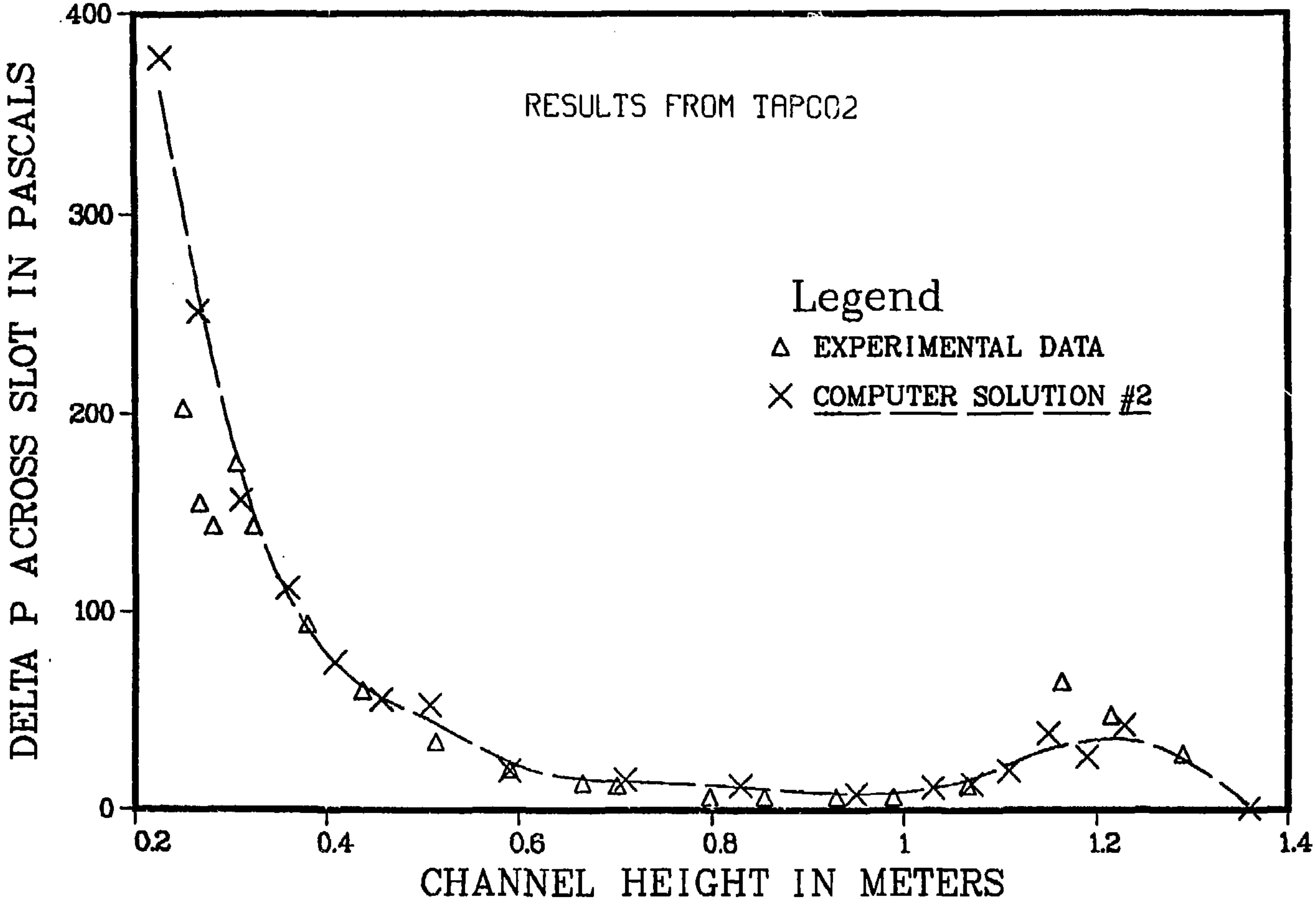

Figure 7

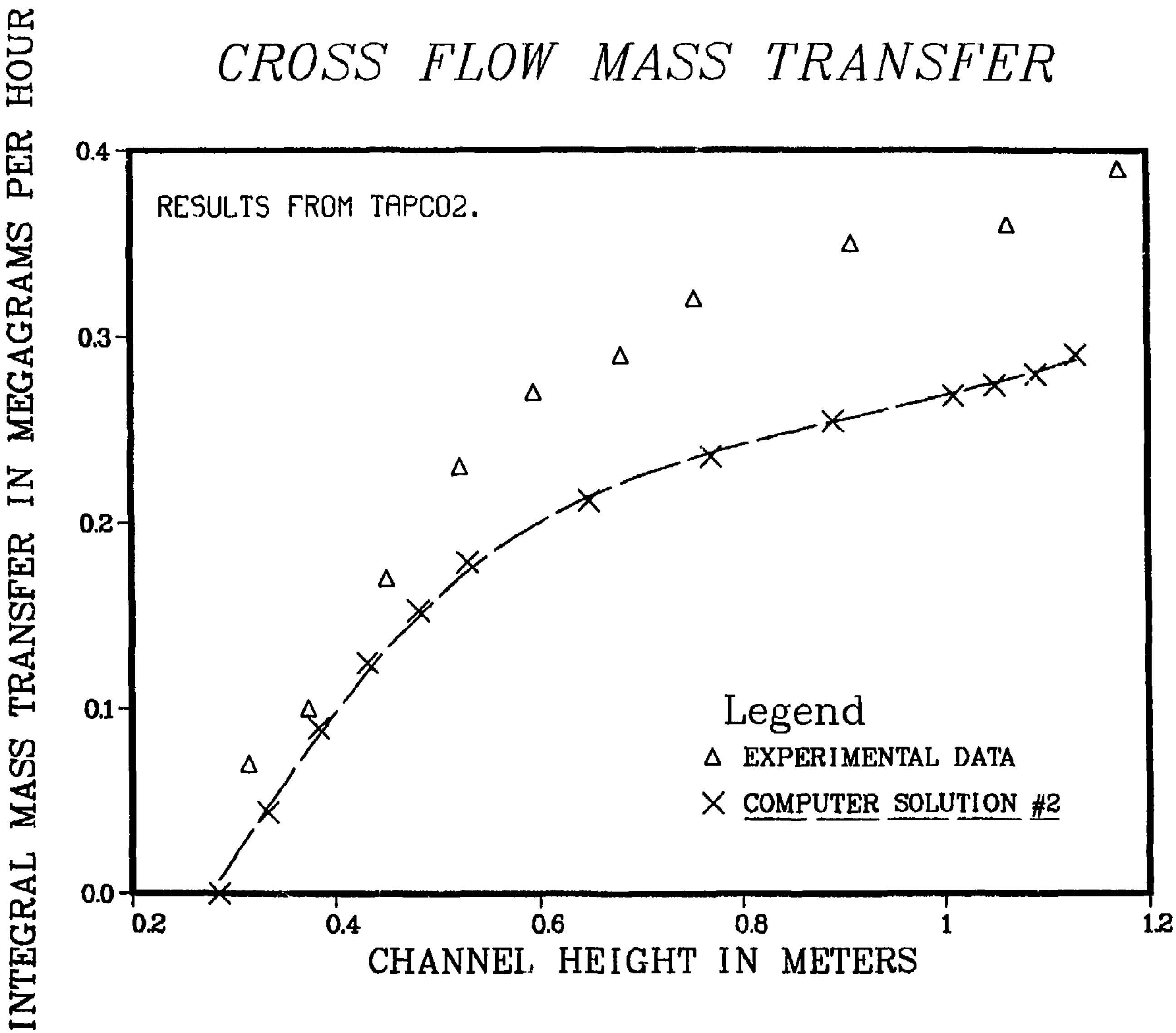
CROSS FLOW MASS TRANSFER
INTEGRAL MASS TRANSFER IN MEGAGRAMS PER HOUR
0.4
0.3
0.2
0.1
0.0
RESULTS FROM TAPCO2.
Legend
EXPERIMENTAL DATA
COMPUTER SOLUTION #2
0.2
0.4
0.6
0.8
1
1.2
CHANNEL HEIGHT IN METERS

Figure 8

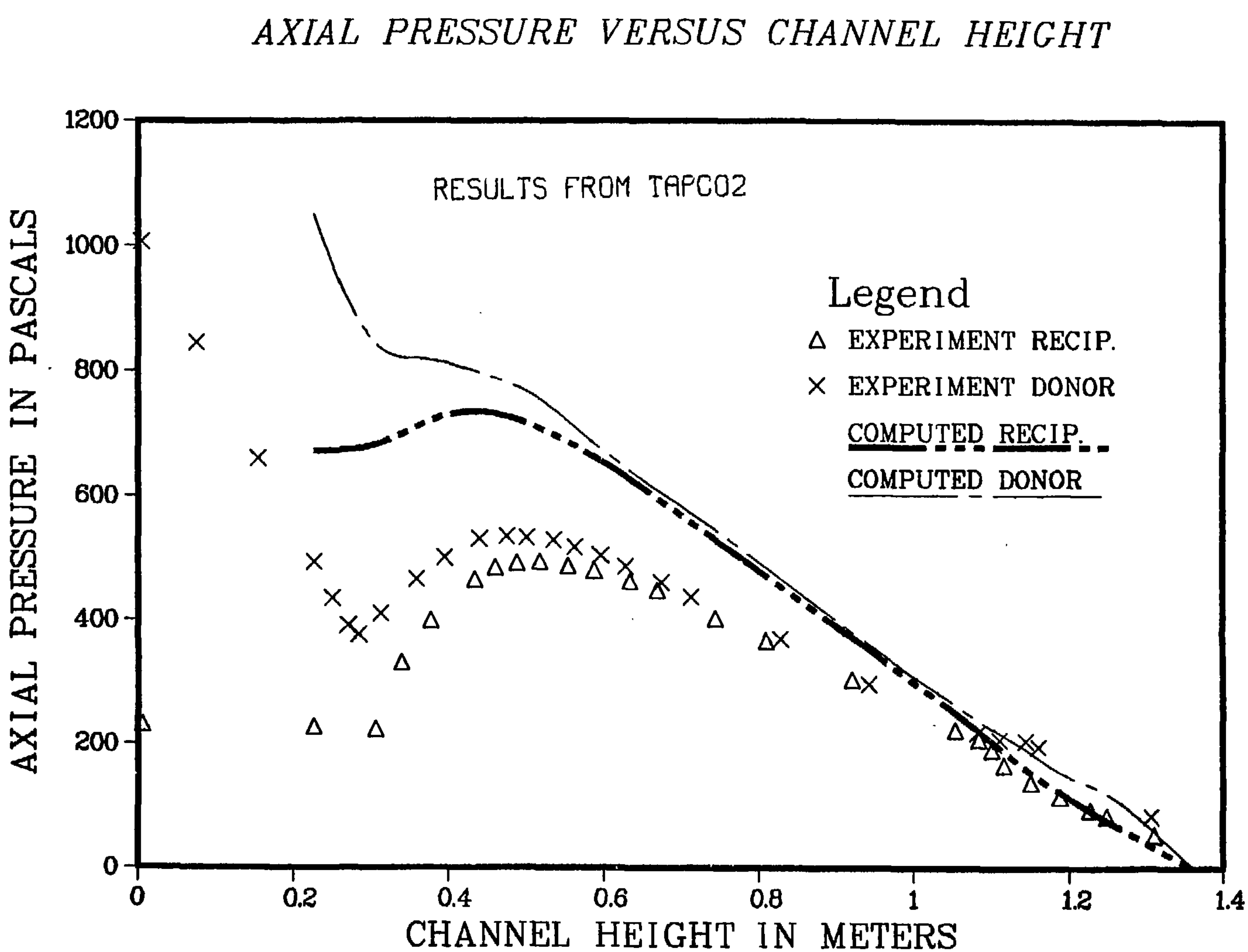
AXIAL PRESSURE VERSUS CHANNEL HEIGHT
RESULTS FROM TAPC02
Legend
EXPERIMENT RECIP.
EXPERIMENT DONOR
COMPUTED RECIP.
COMPUTED DONOR
AXIAL PRESSURE IN PASCALS
0
200
400
600
800
1000
1200
CHANNEL HEIGHT IN METERS
0
0.2
0.4
0.6
0.8
1
1.2
1.4

Figure 9

DONOR VELOCITY VERSUS CHANNEL HEIGHT

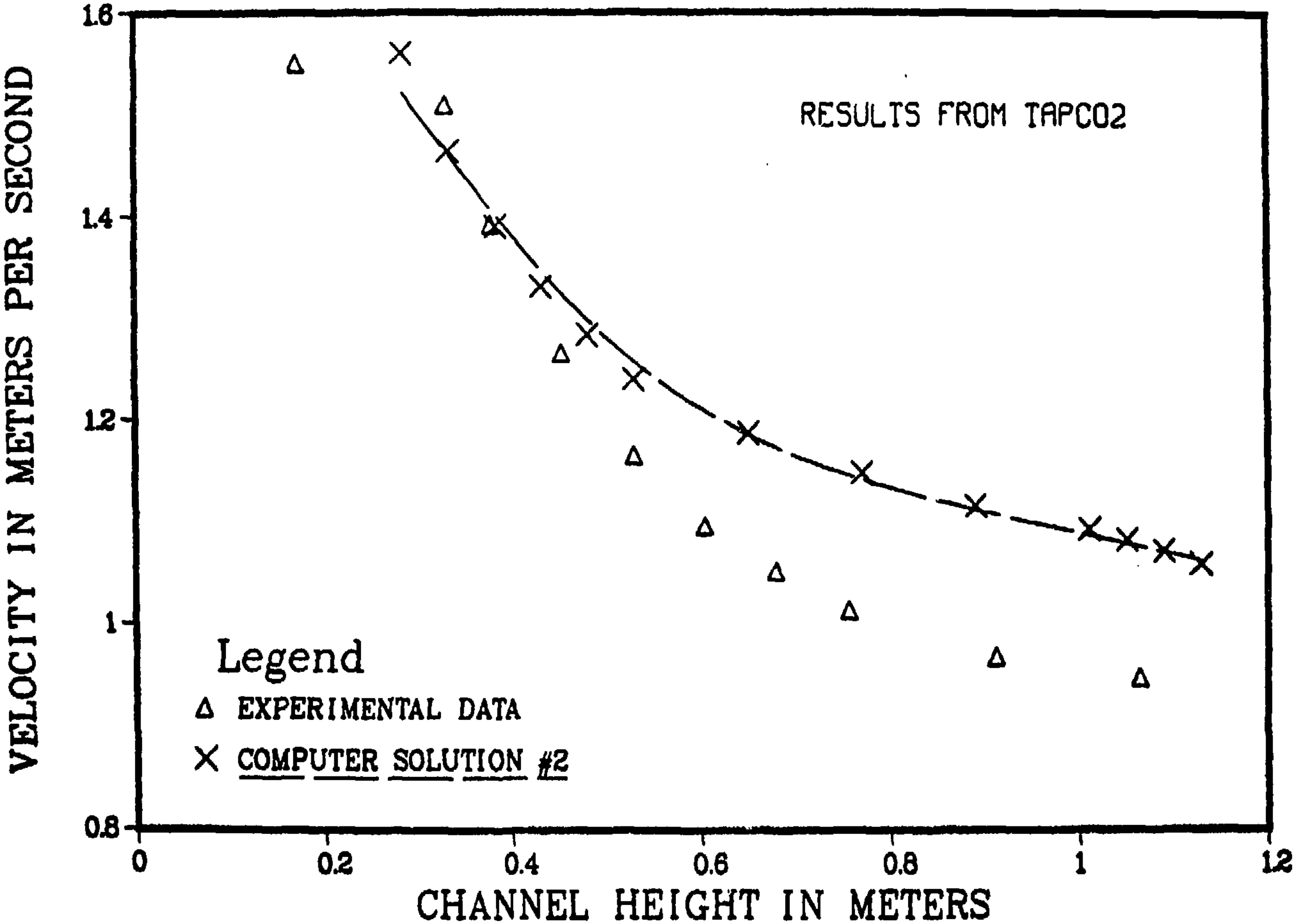

Figure 10

Figure 11

TRANSVERSE RESISTANCE COEFFICIENT

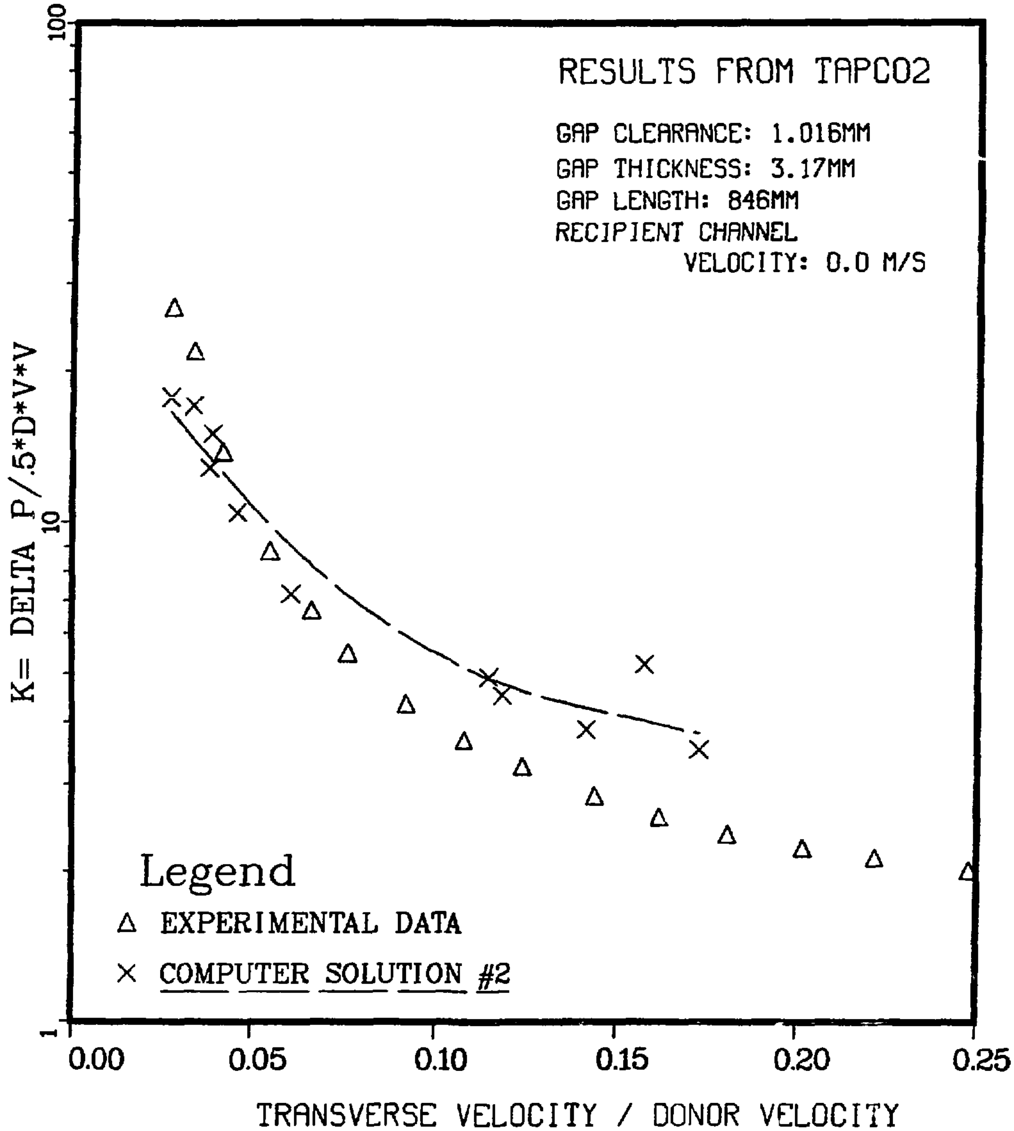

Figure 12

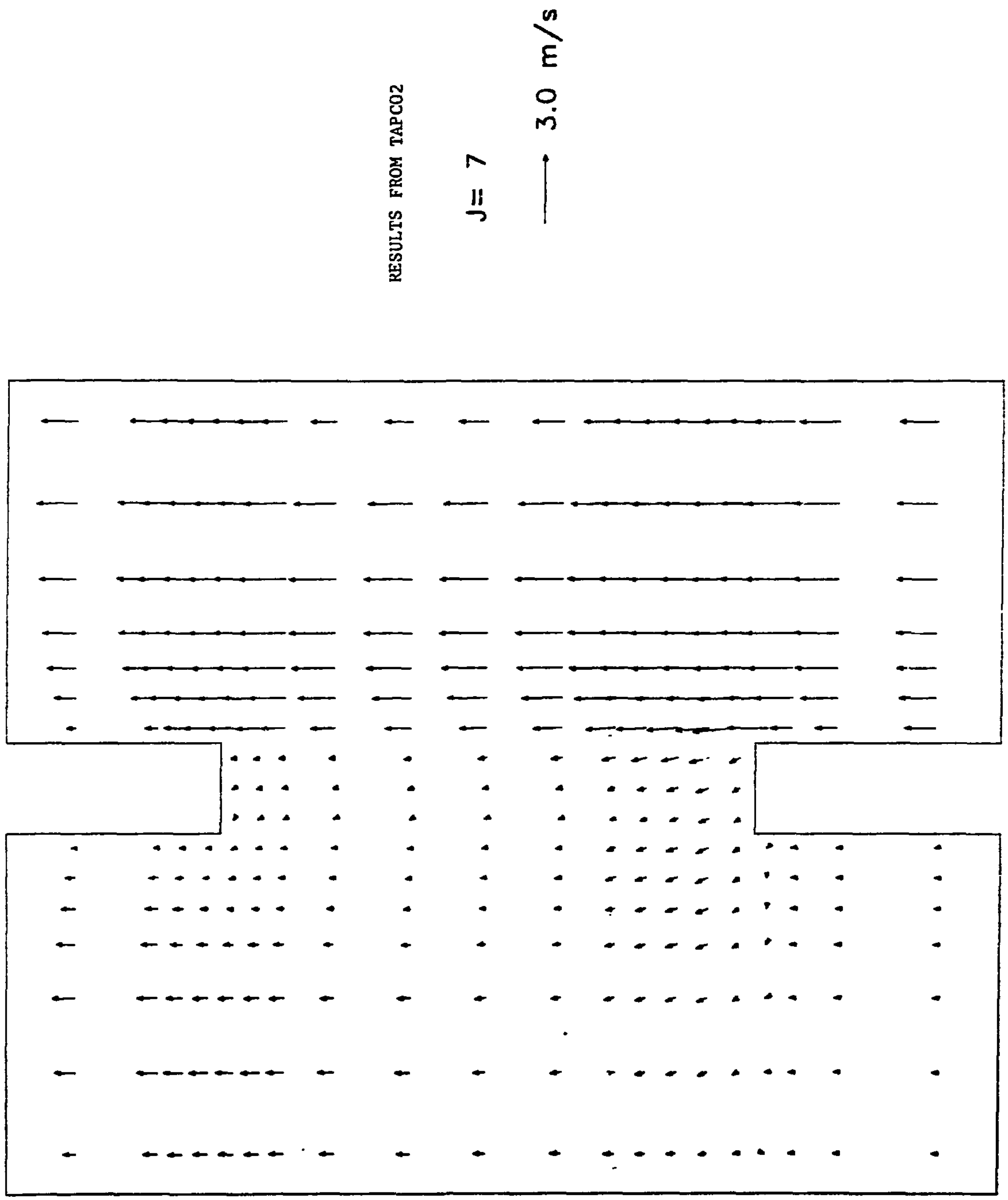

Figure 13

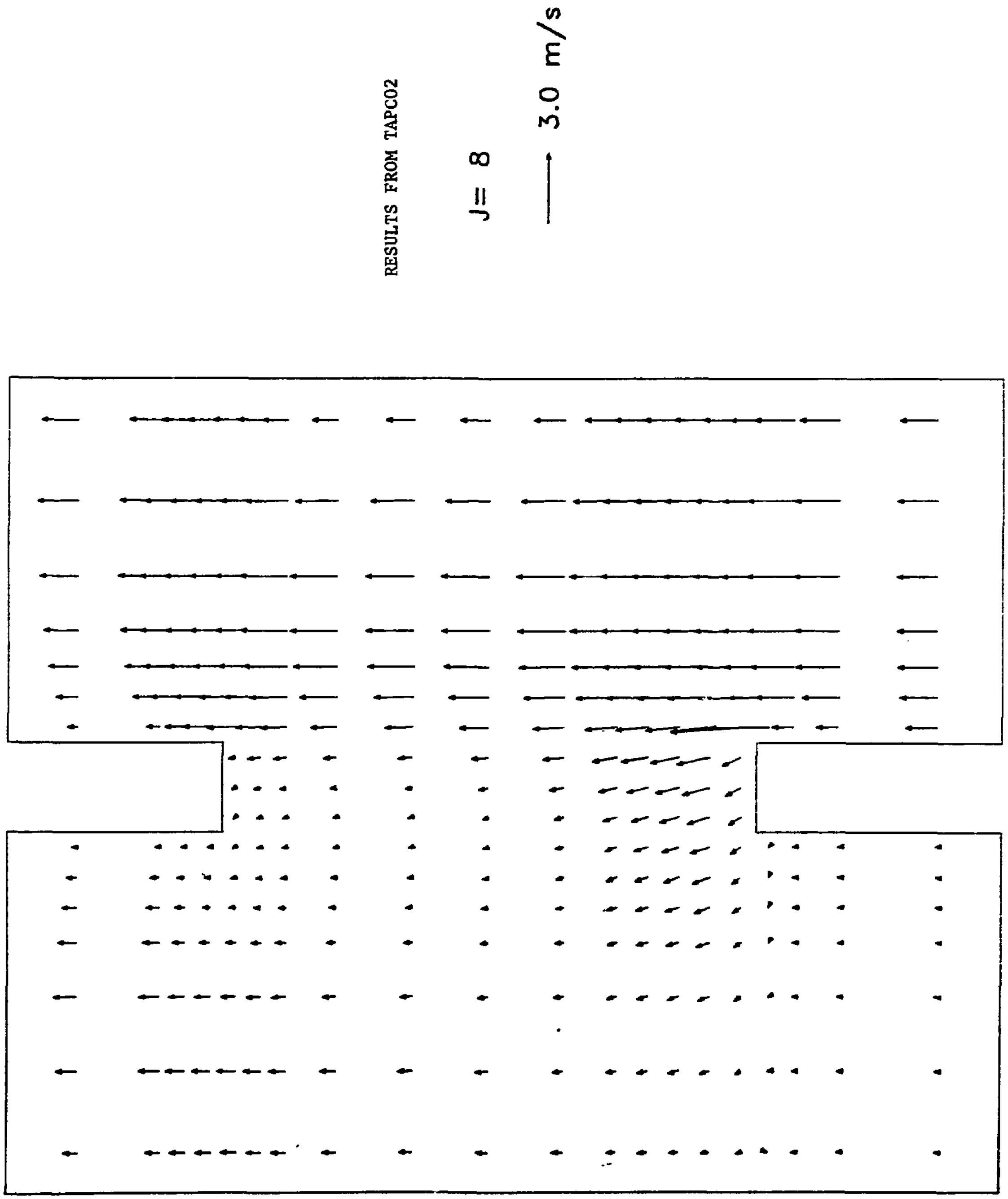

Figure 14

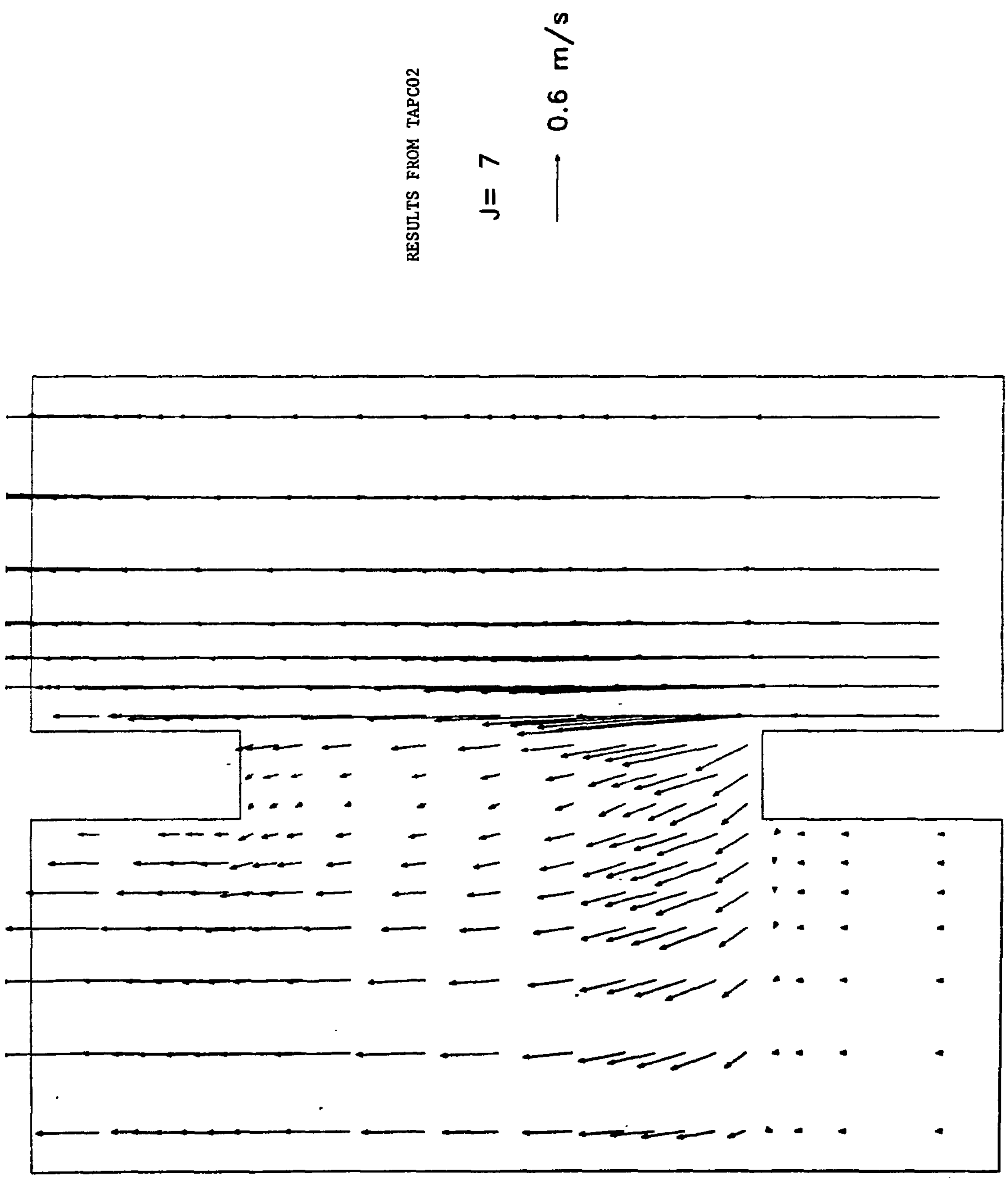

Figure 15

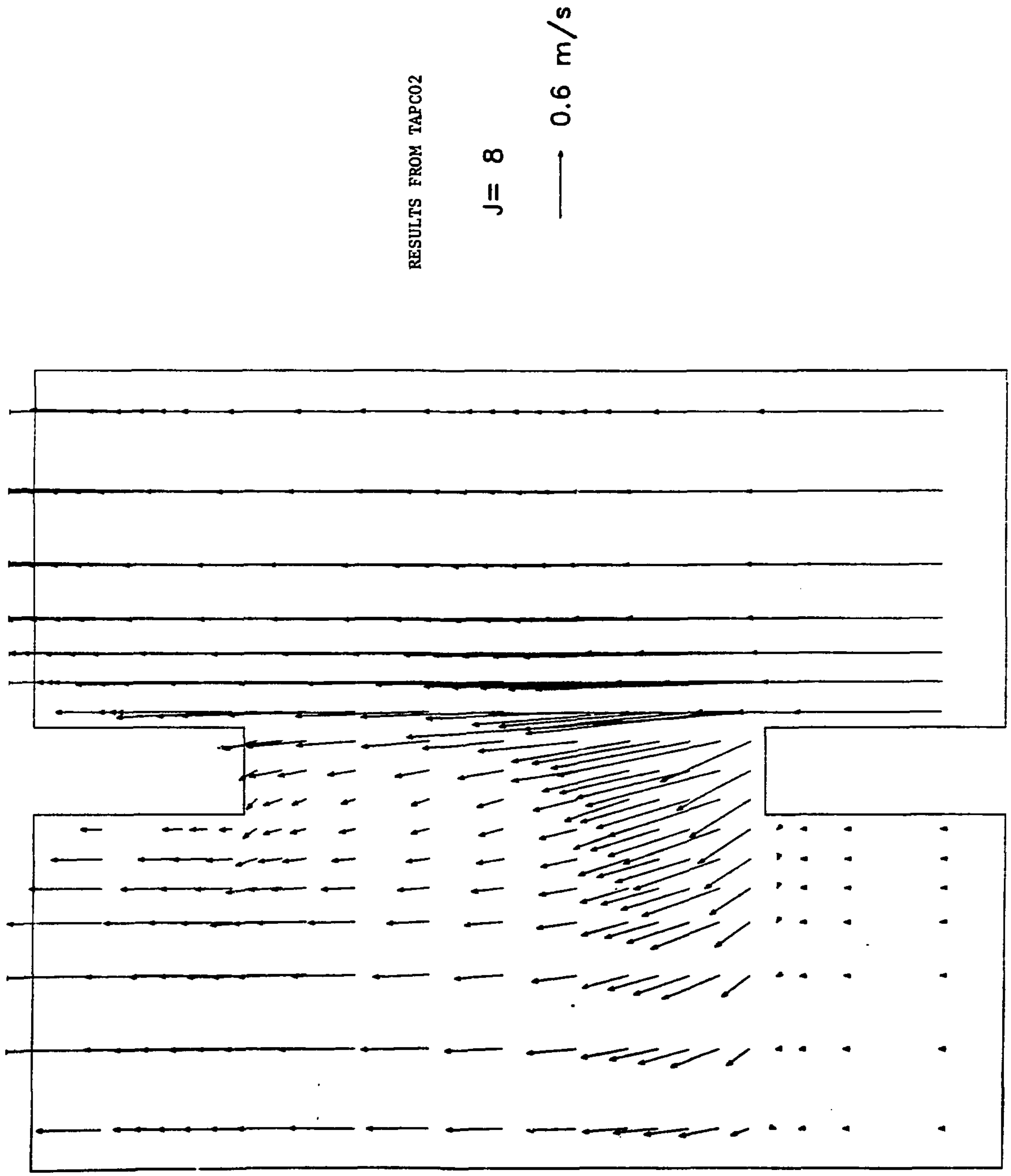

Figure 16

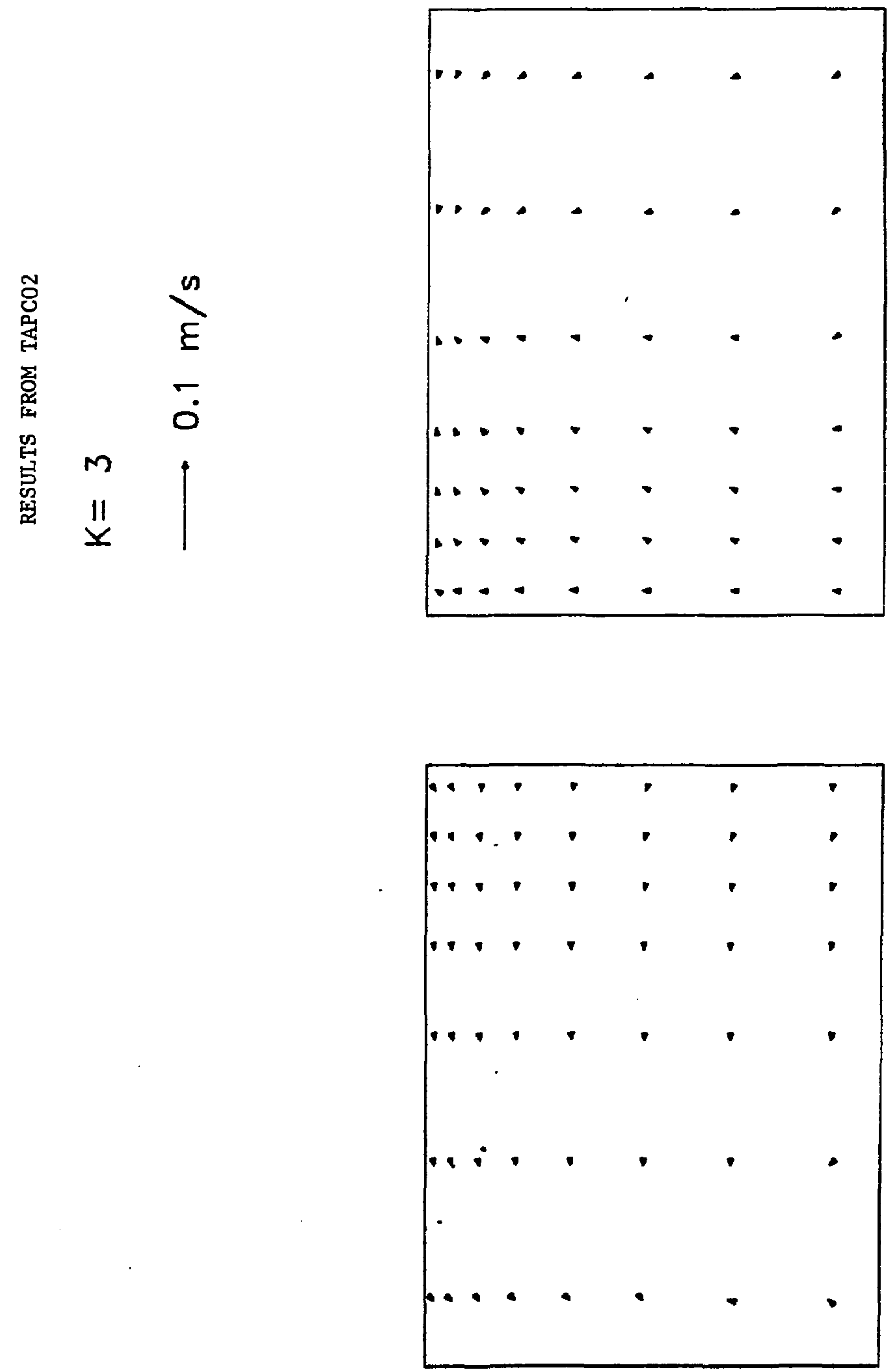

Figure 17

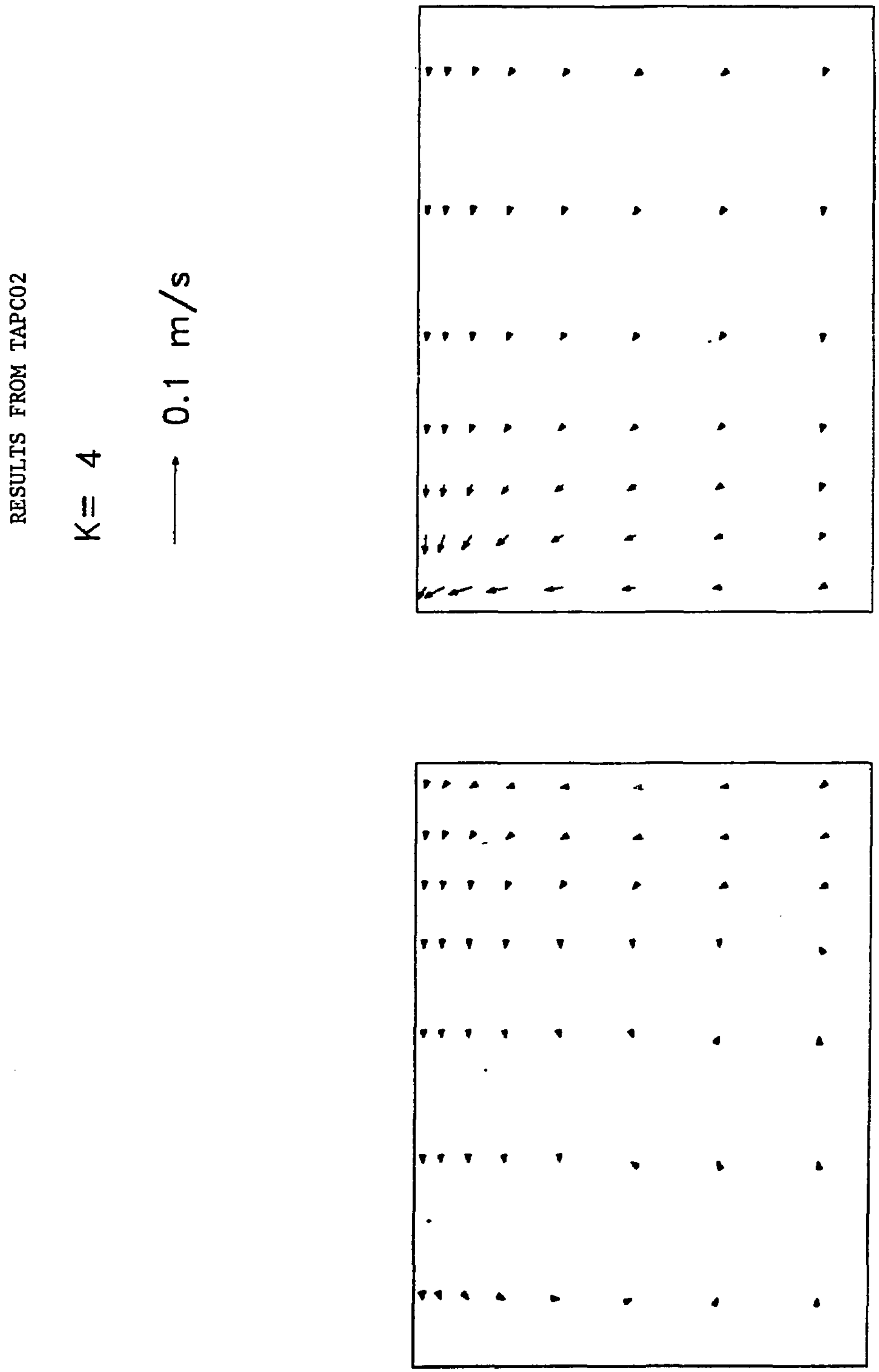

Figure 18

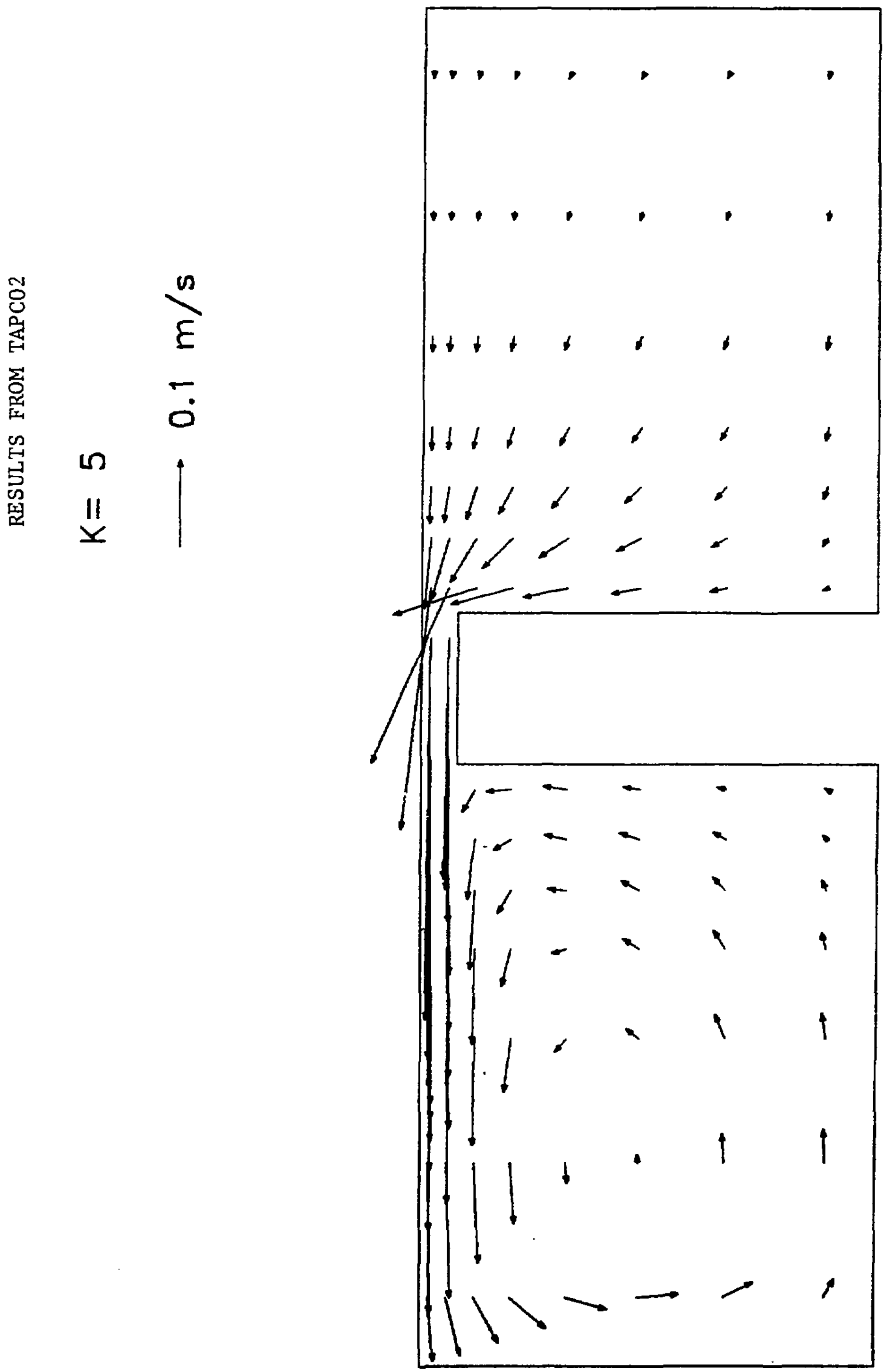

Figure 19

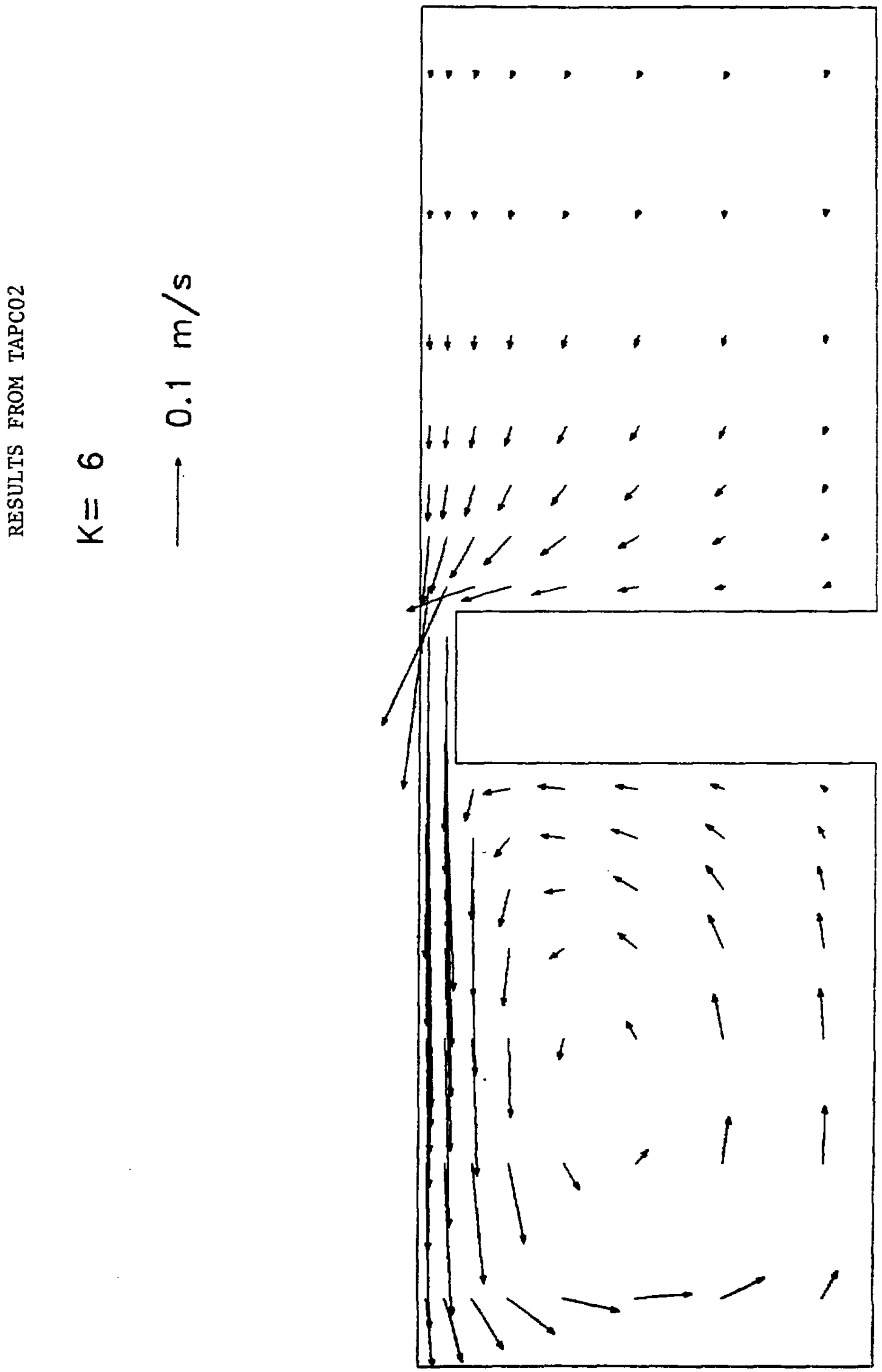

Figure 20

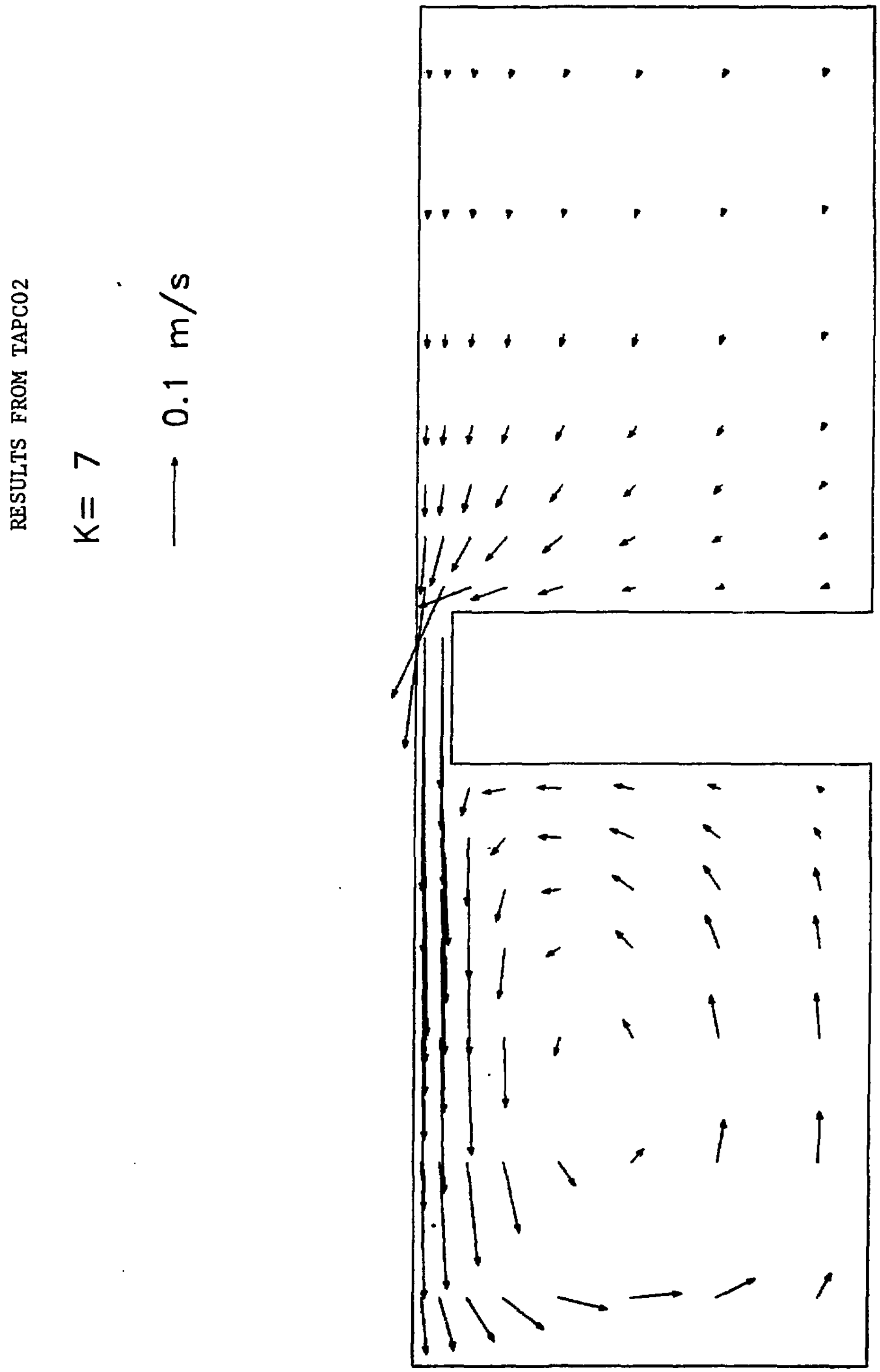

Figure 21

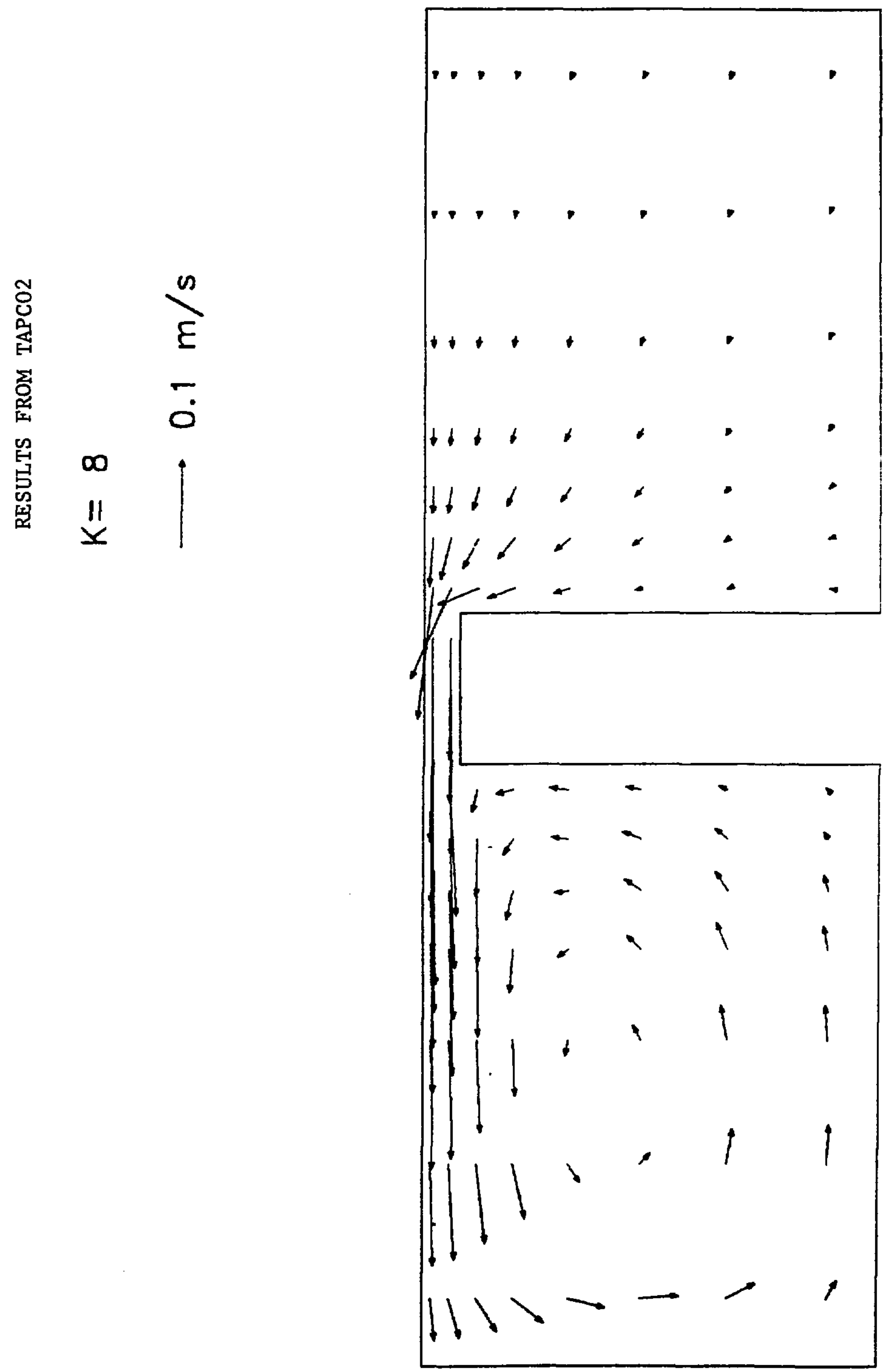

Figure 22

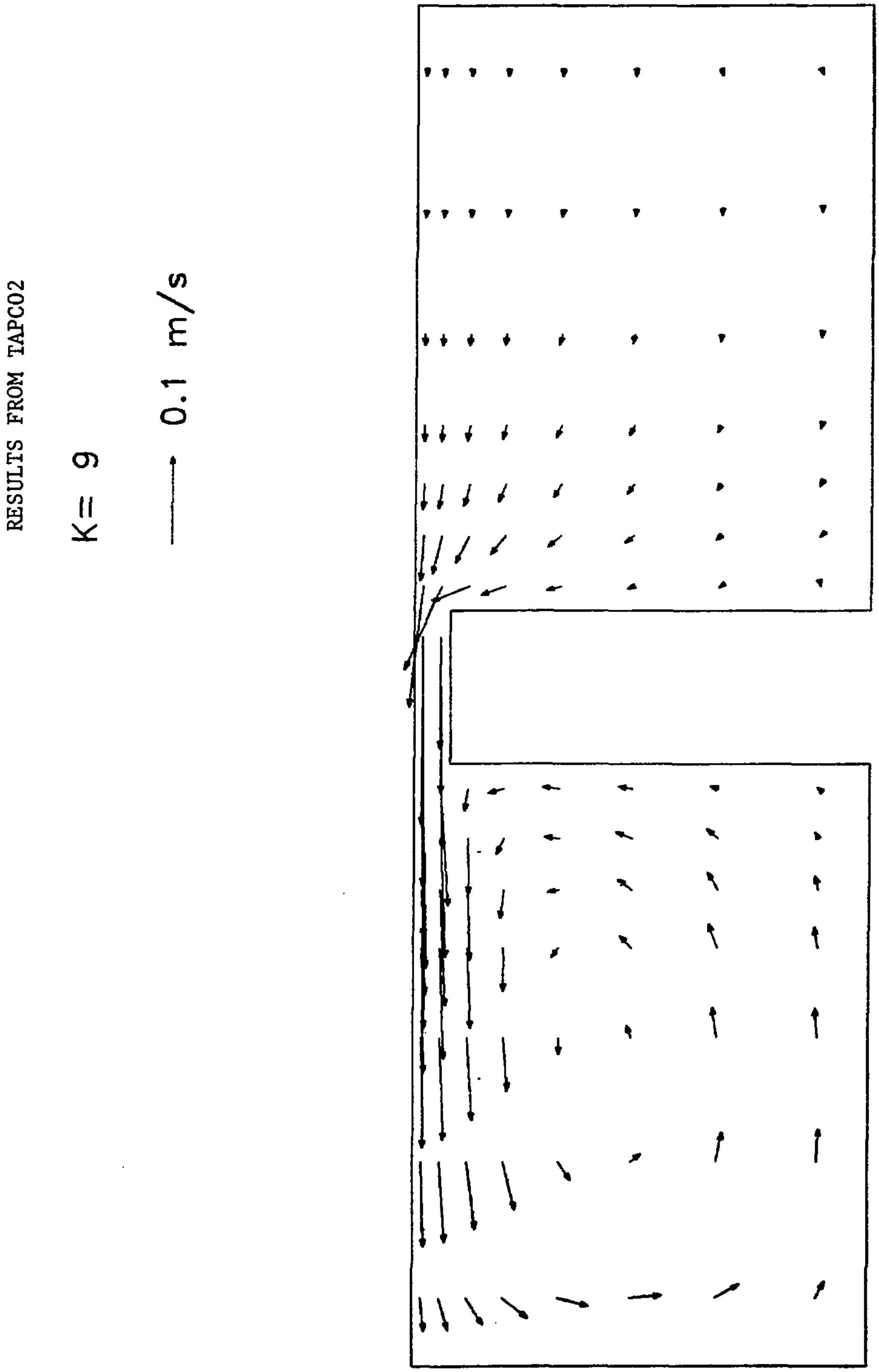

Figure 23

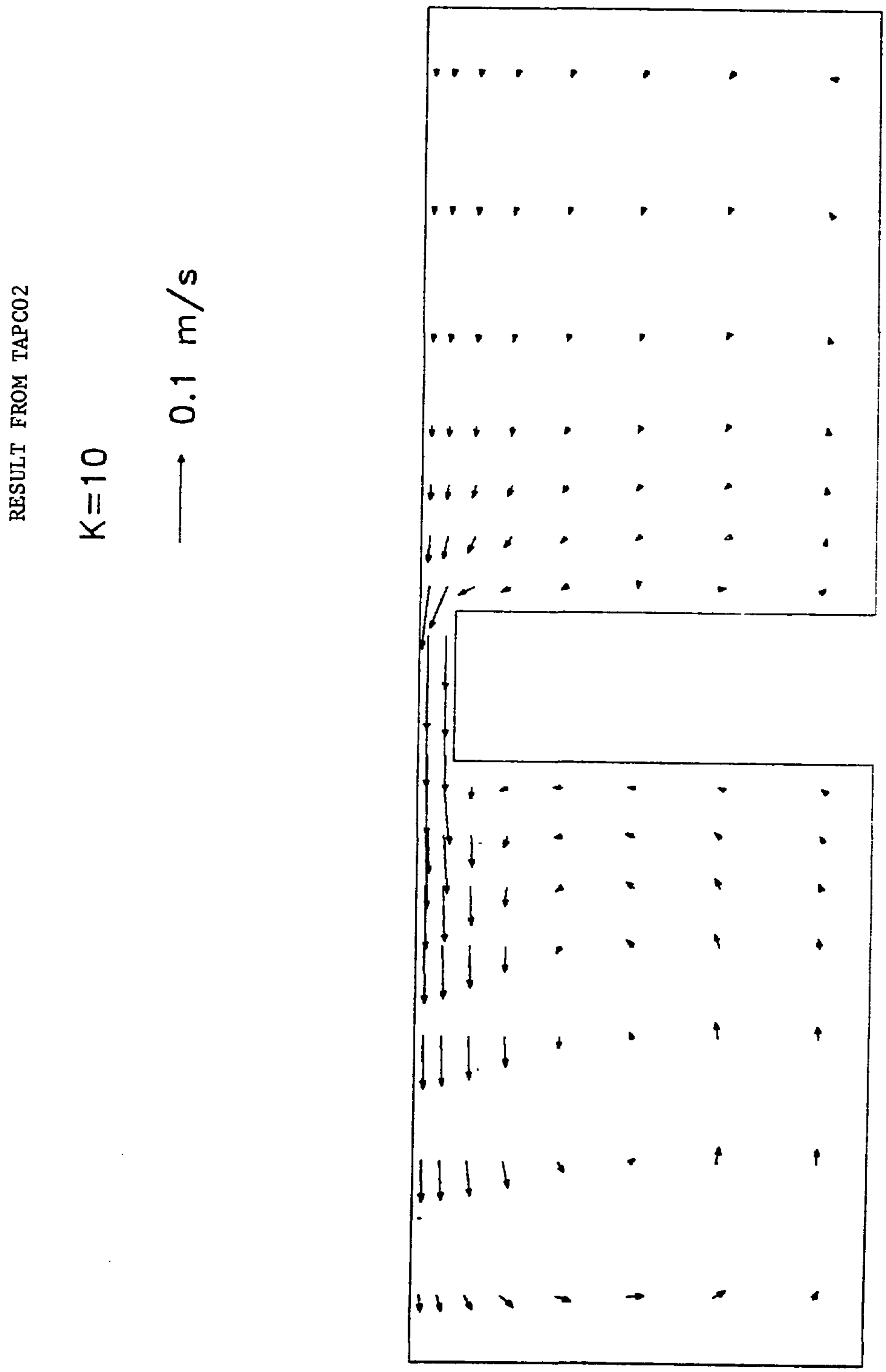

Figure 24

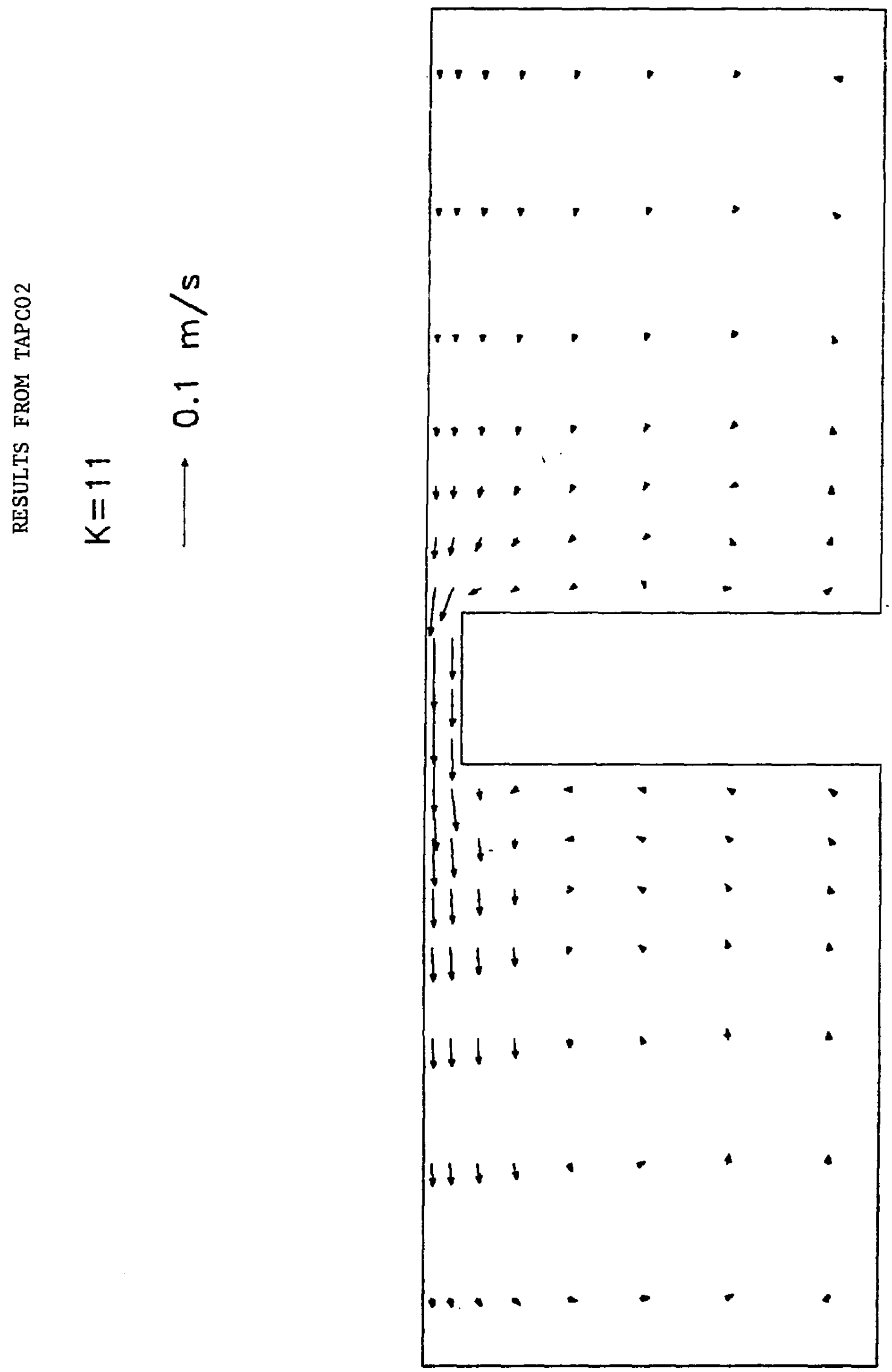

Figure 25

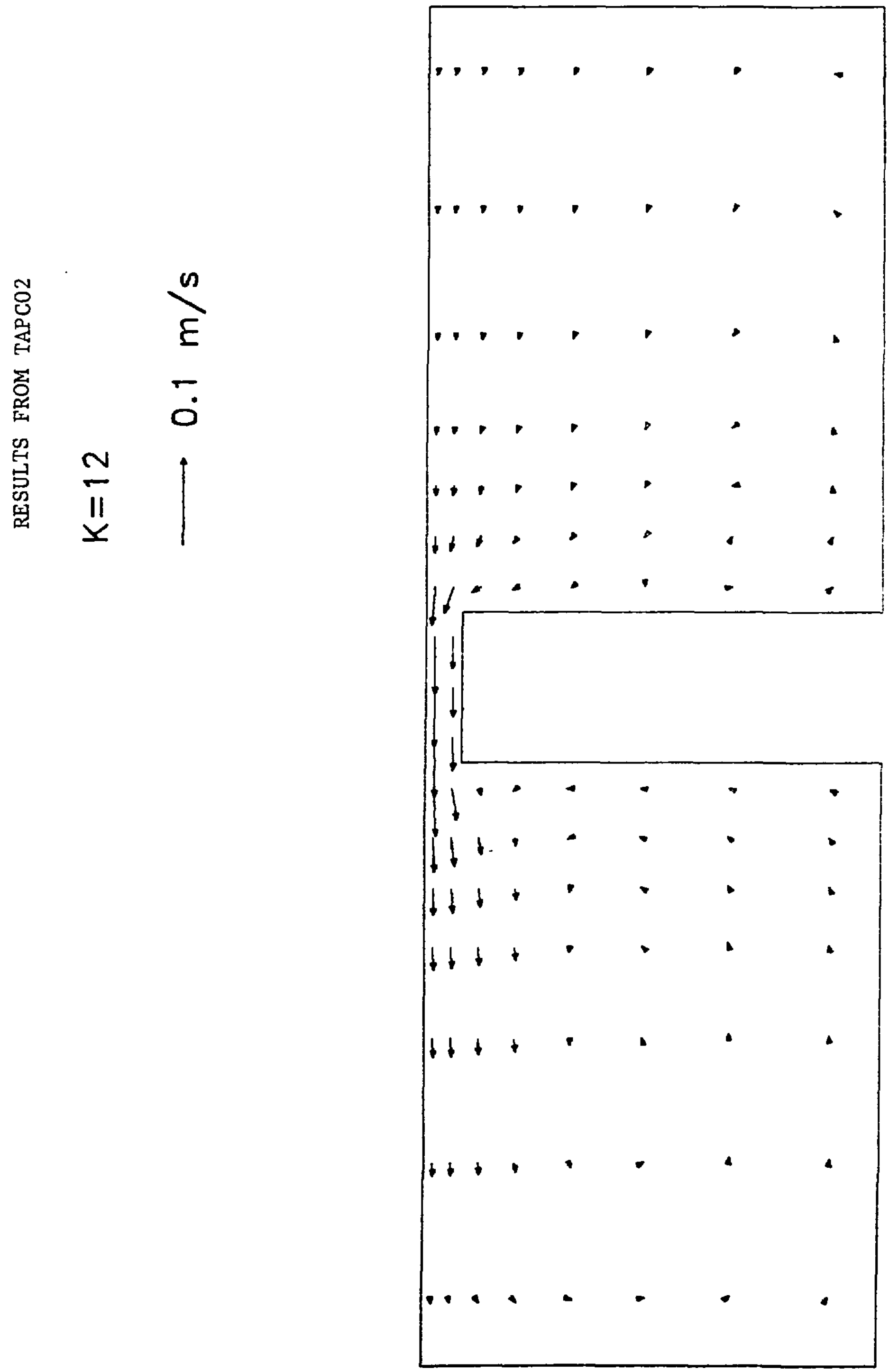

Figure 26

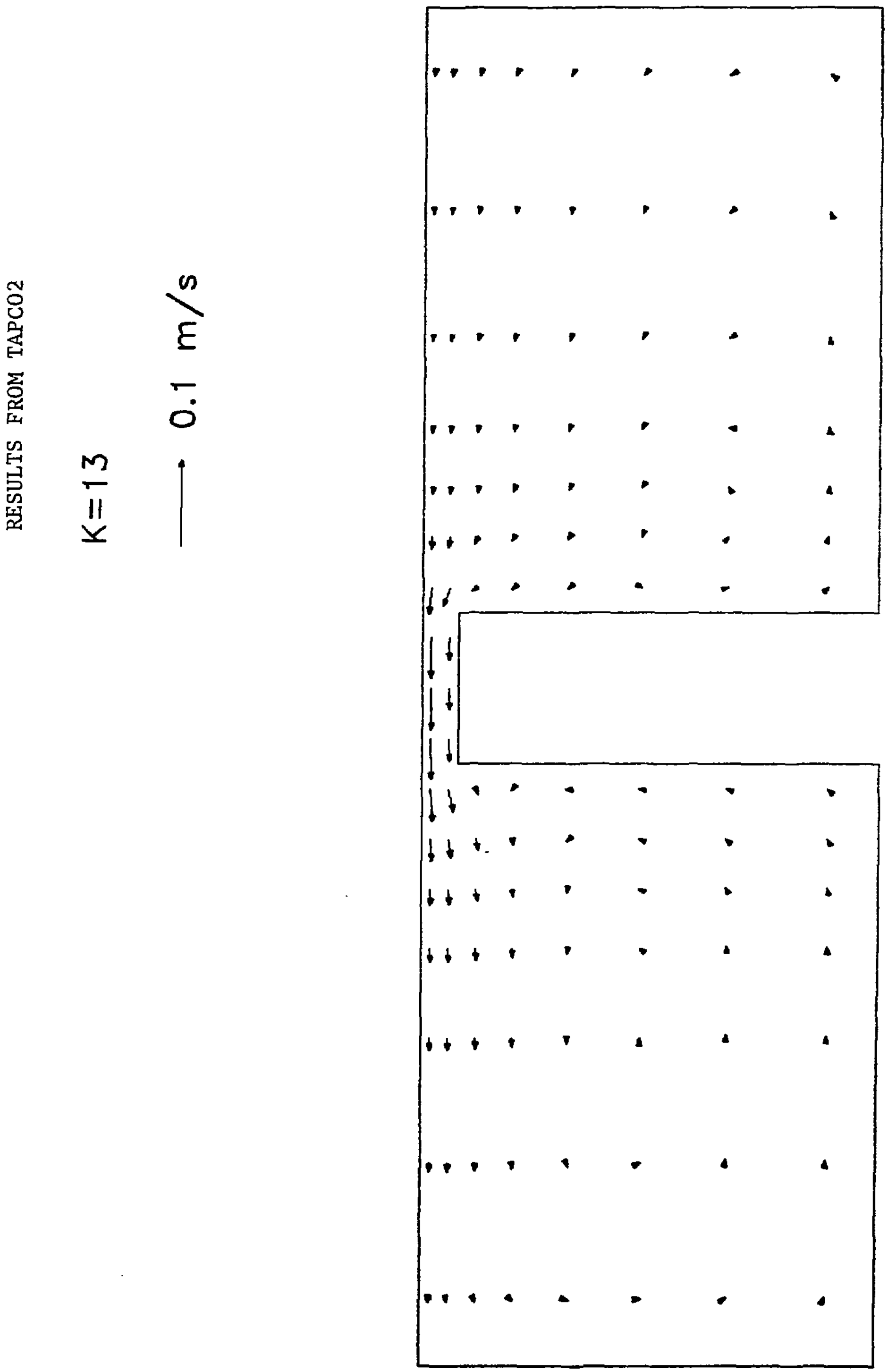

Figure 27

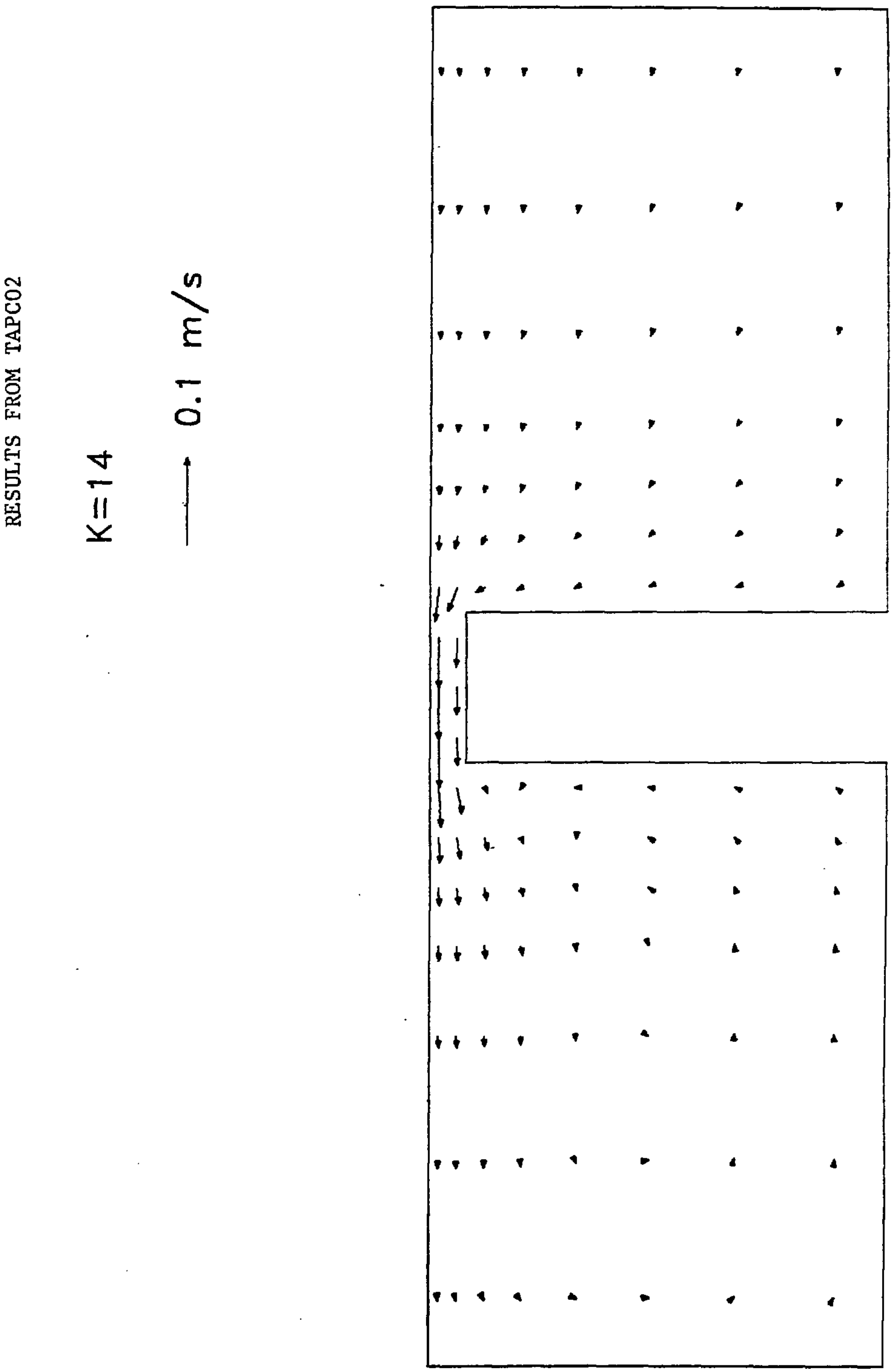

Figure 28

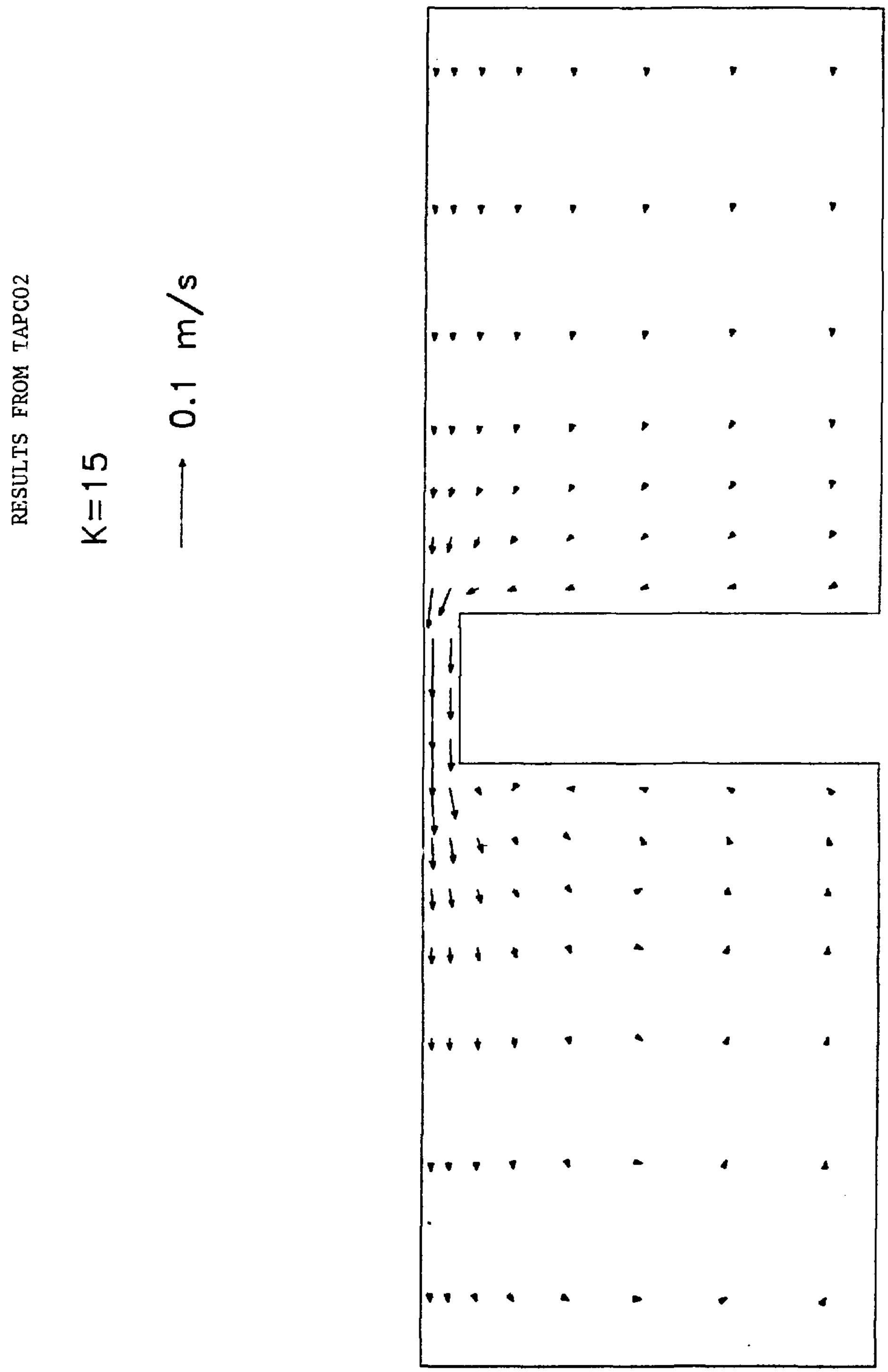

Figure 29

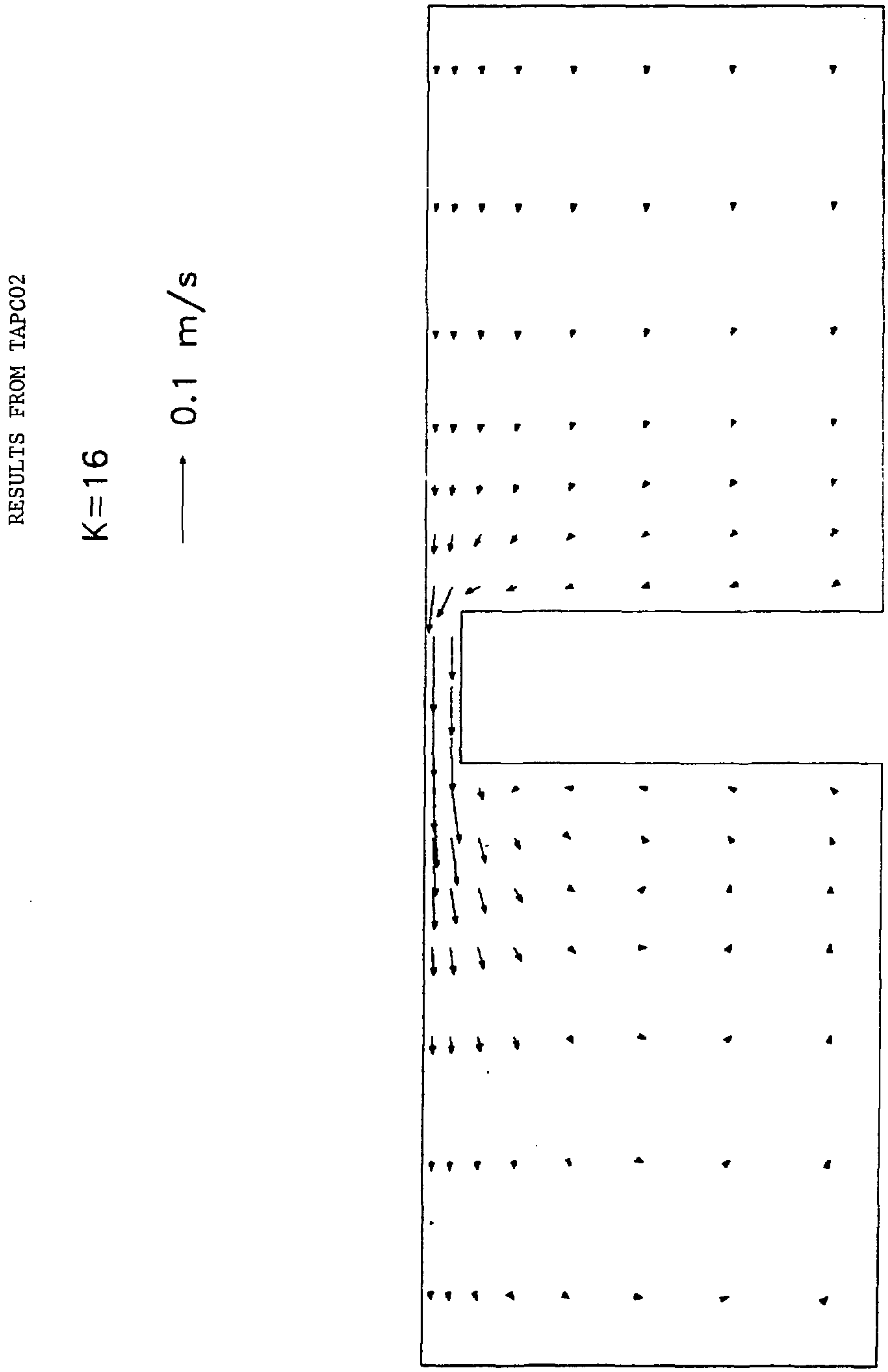

Figure 30

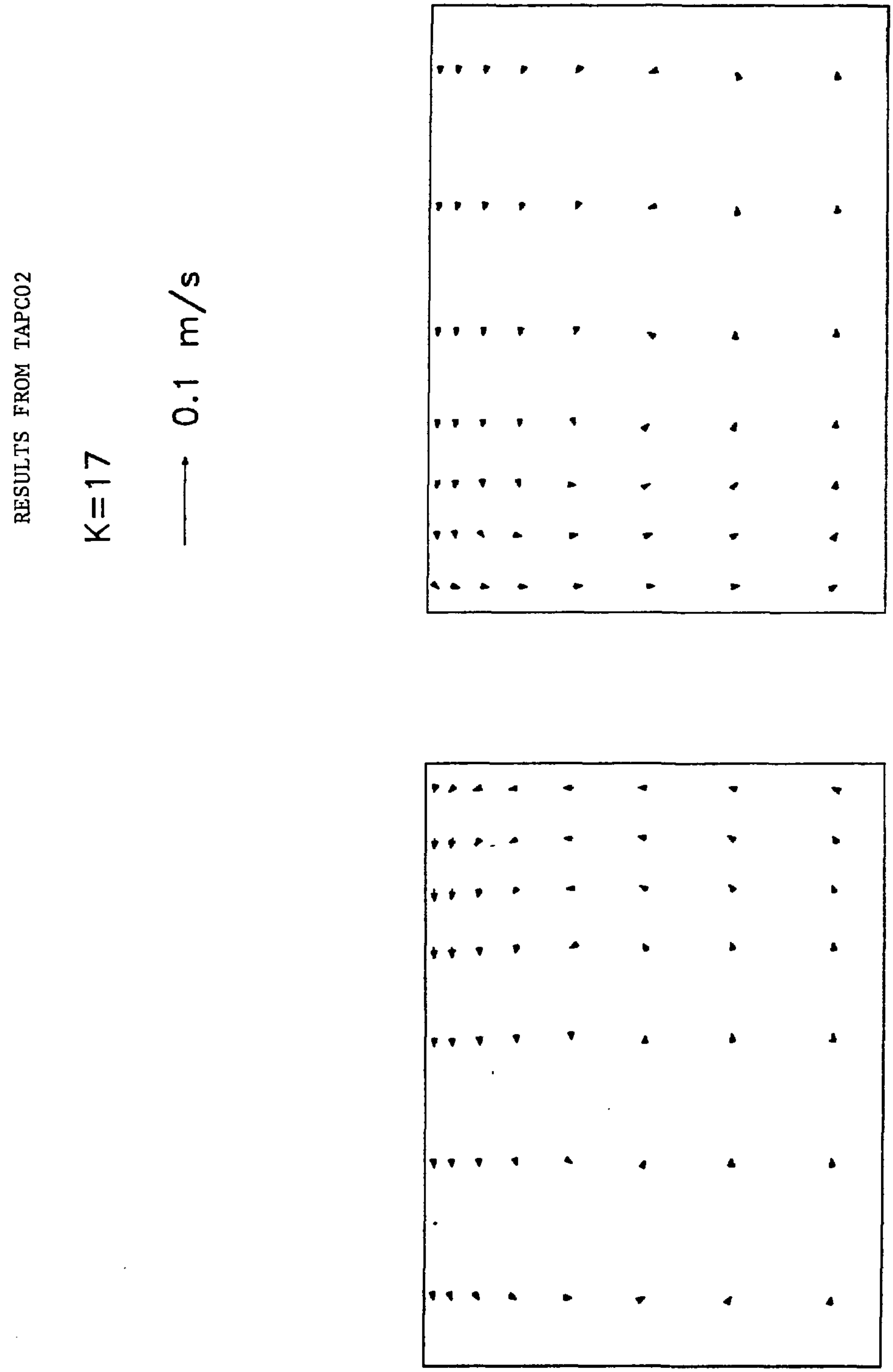

Figure 31

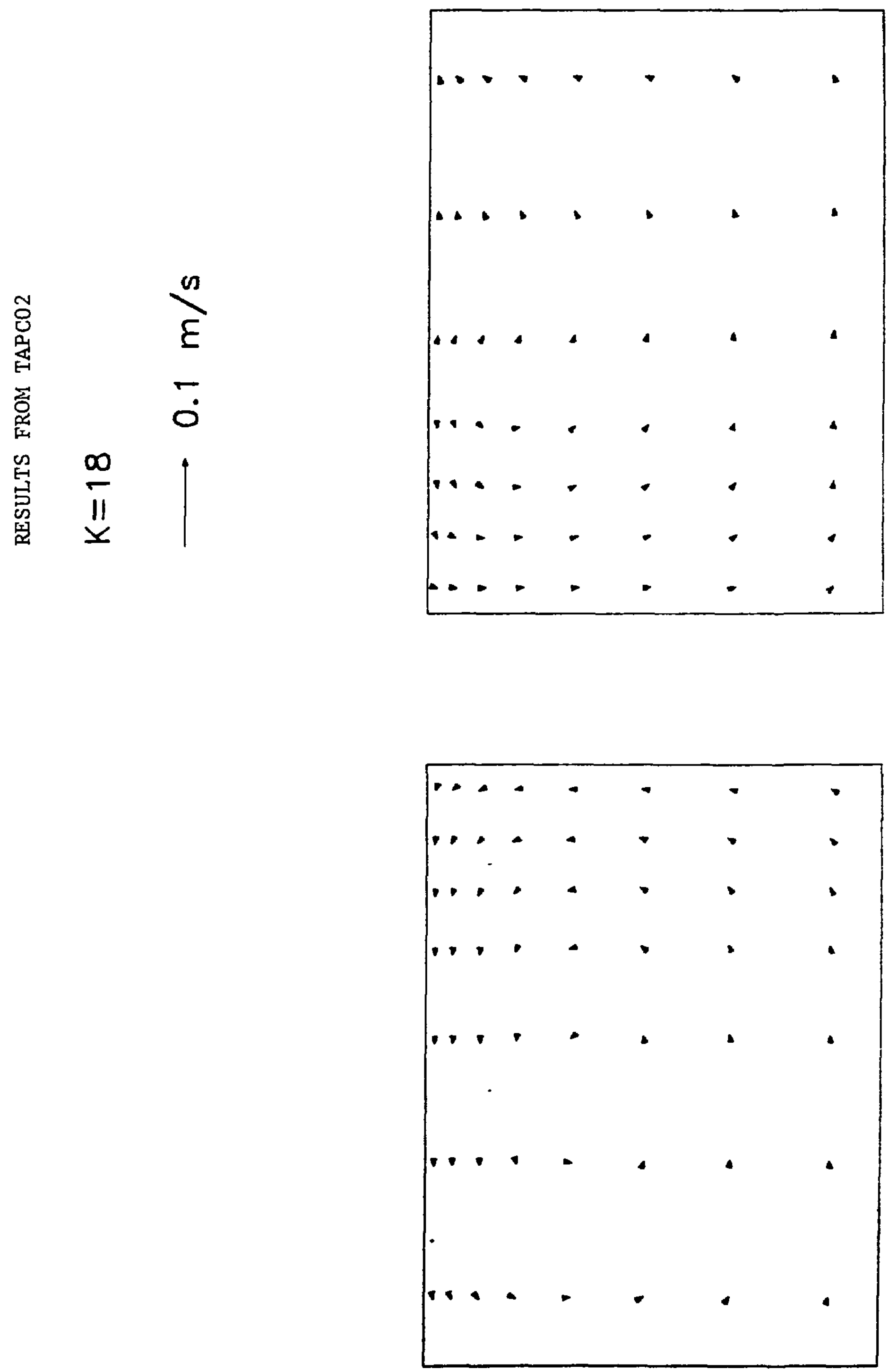

Figure 32

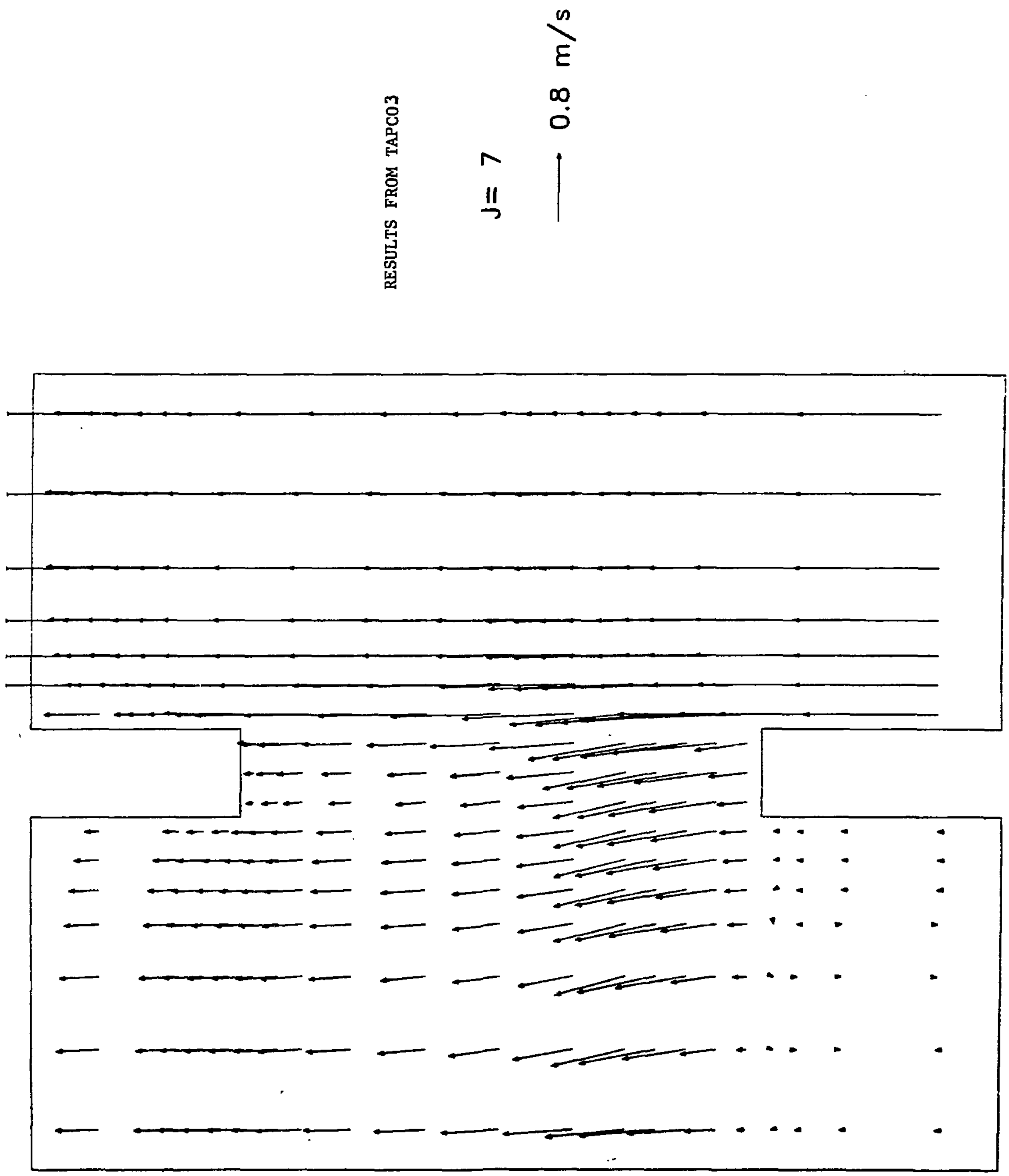

Figure 33

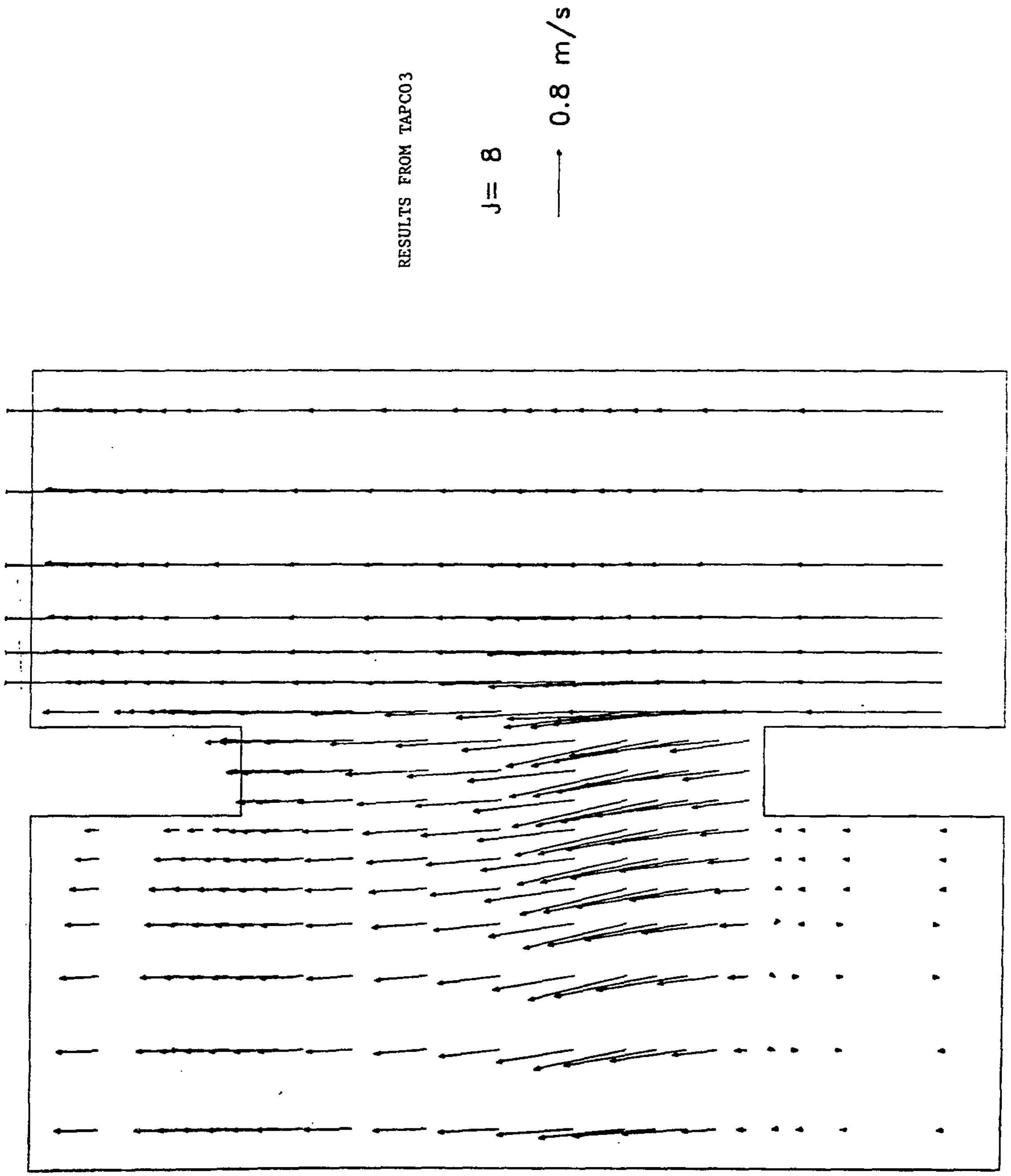

Figure 34

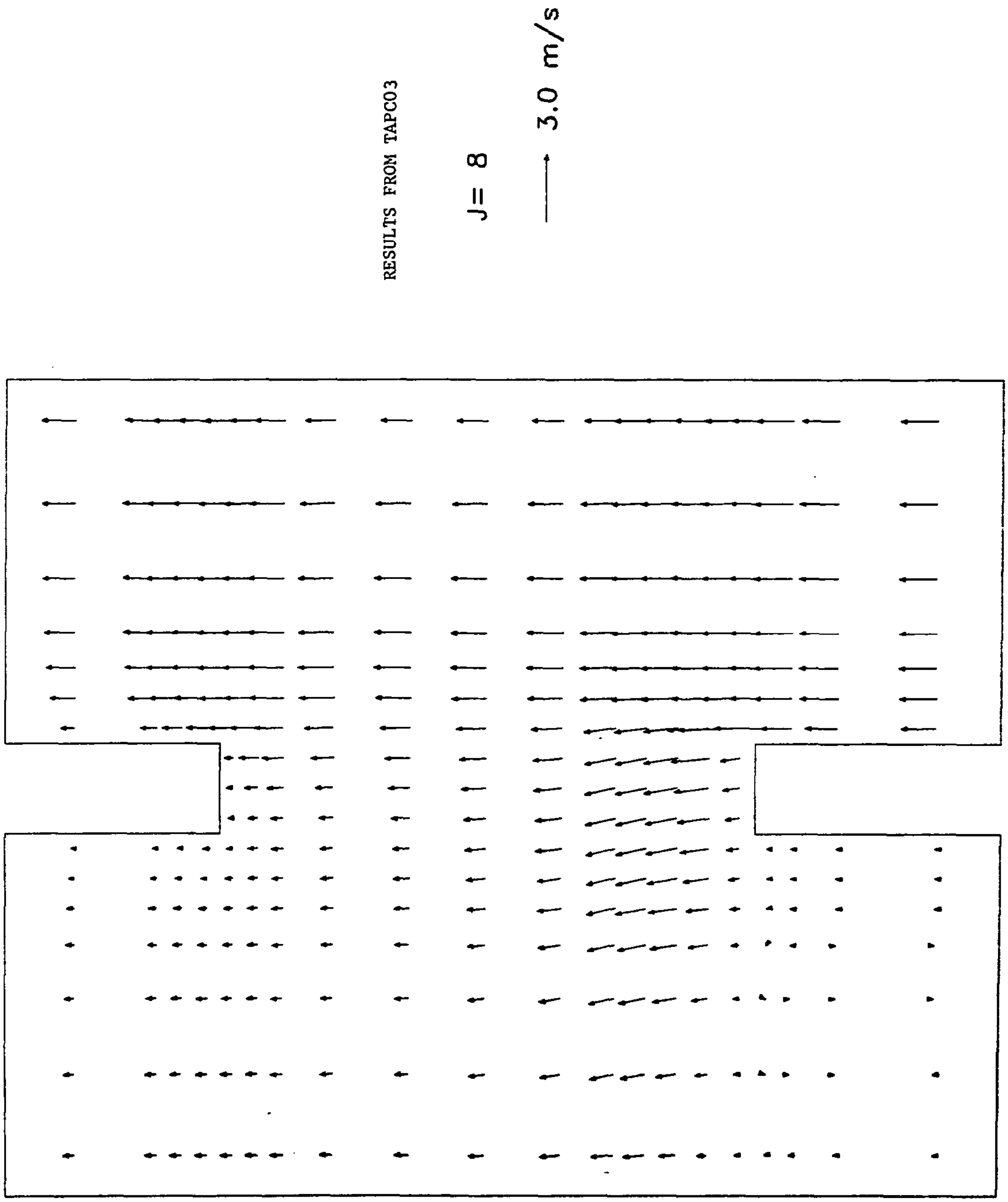

Figure 35

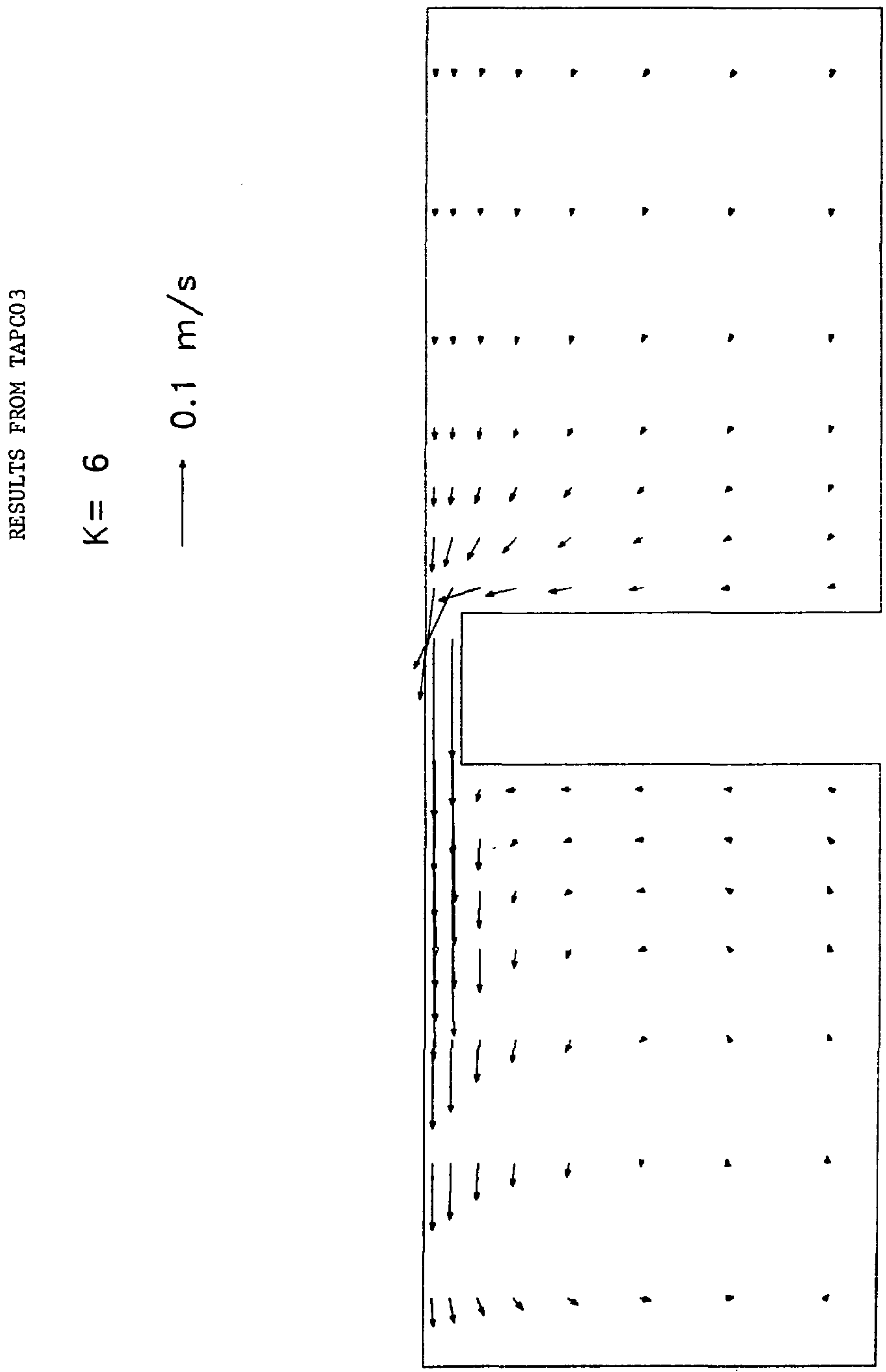

Figure 36

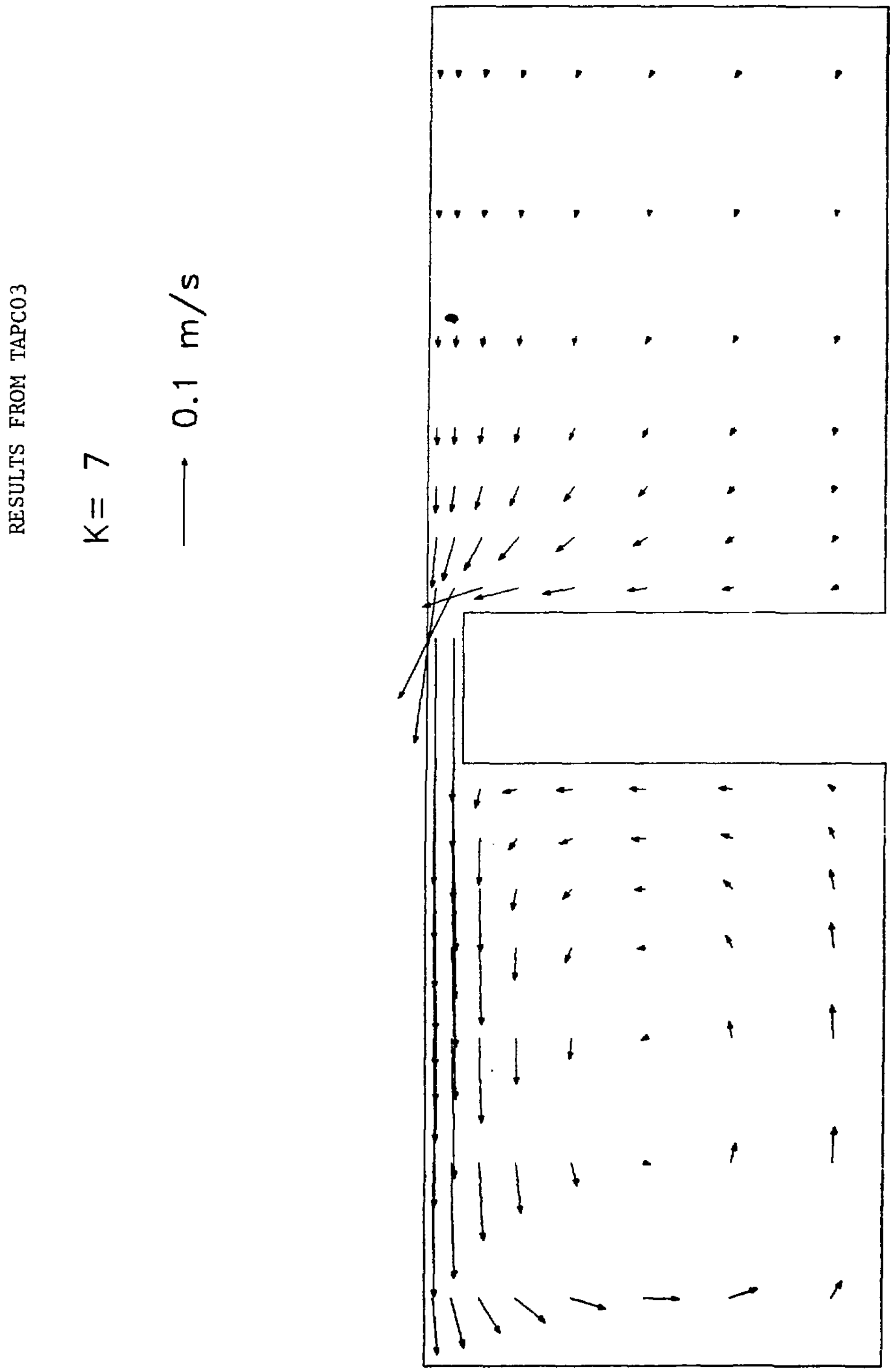

Figure 37

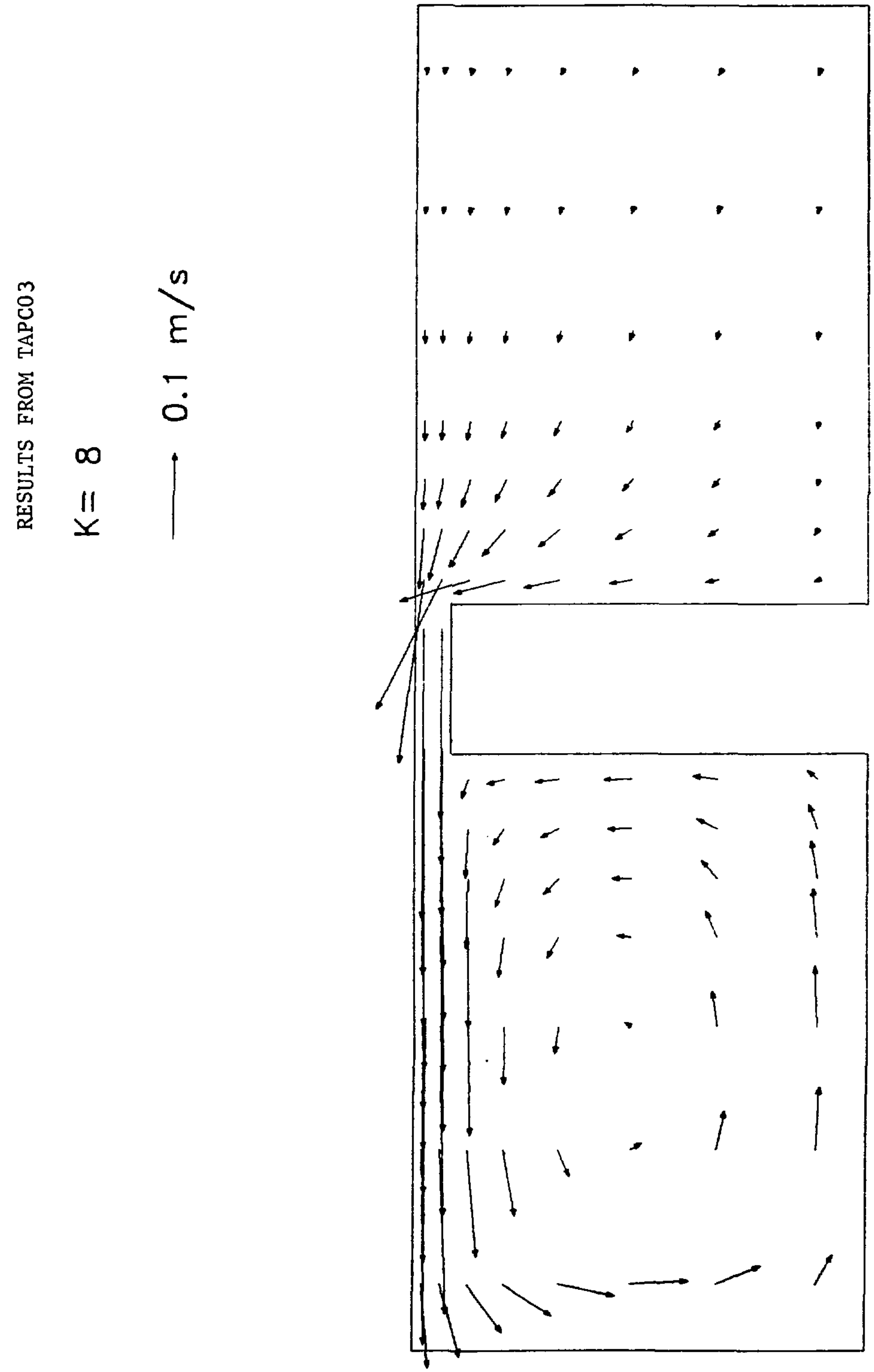

Figure 38

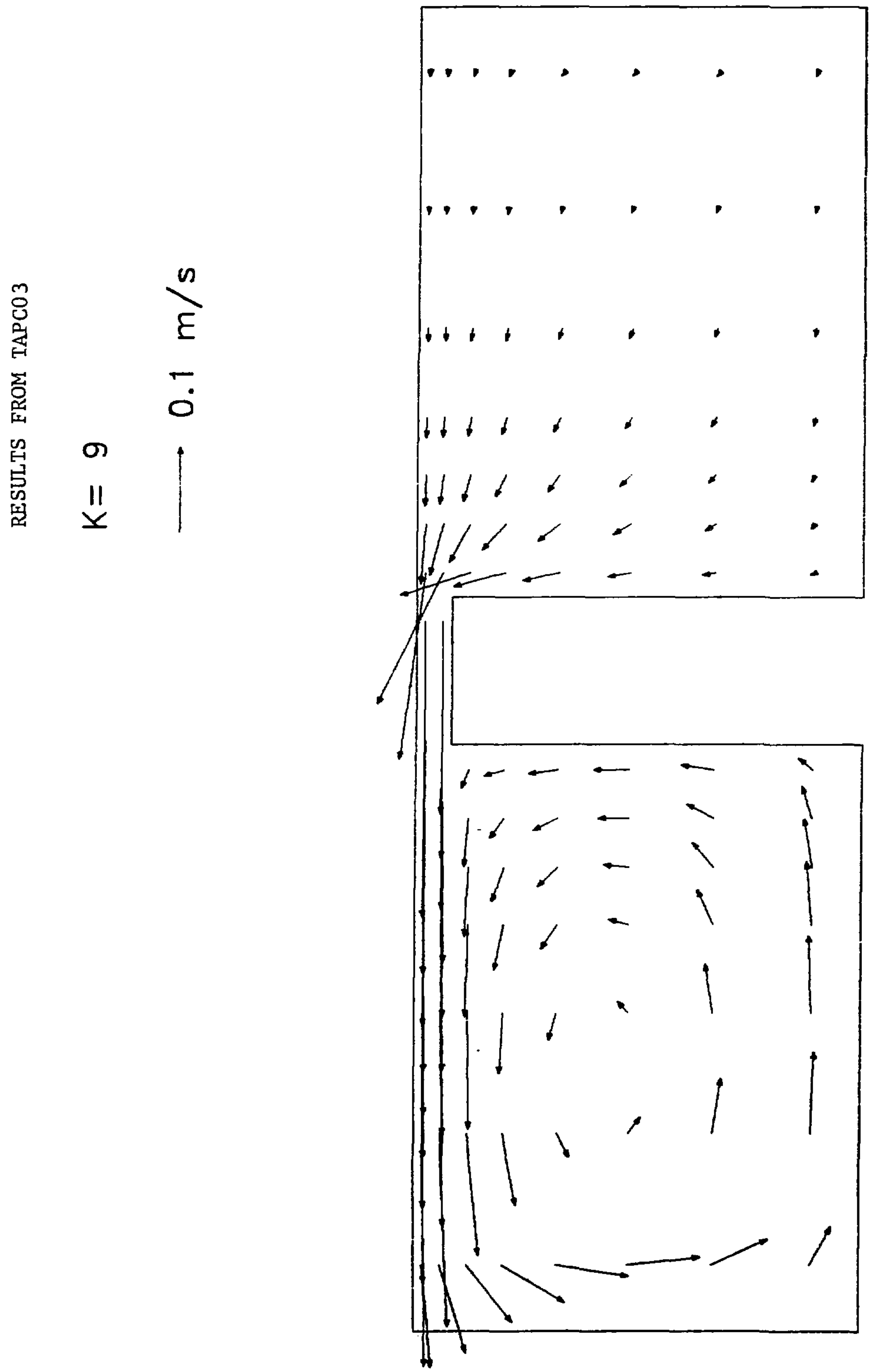

Figure 39

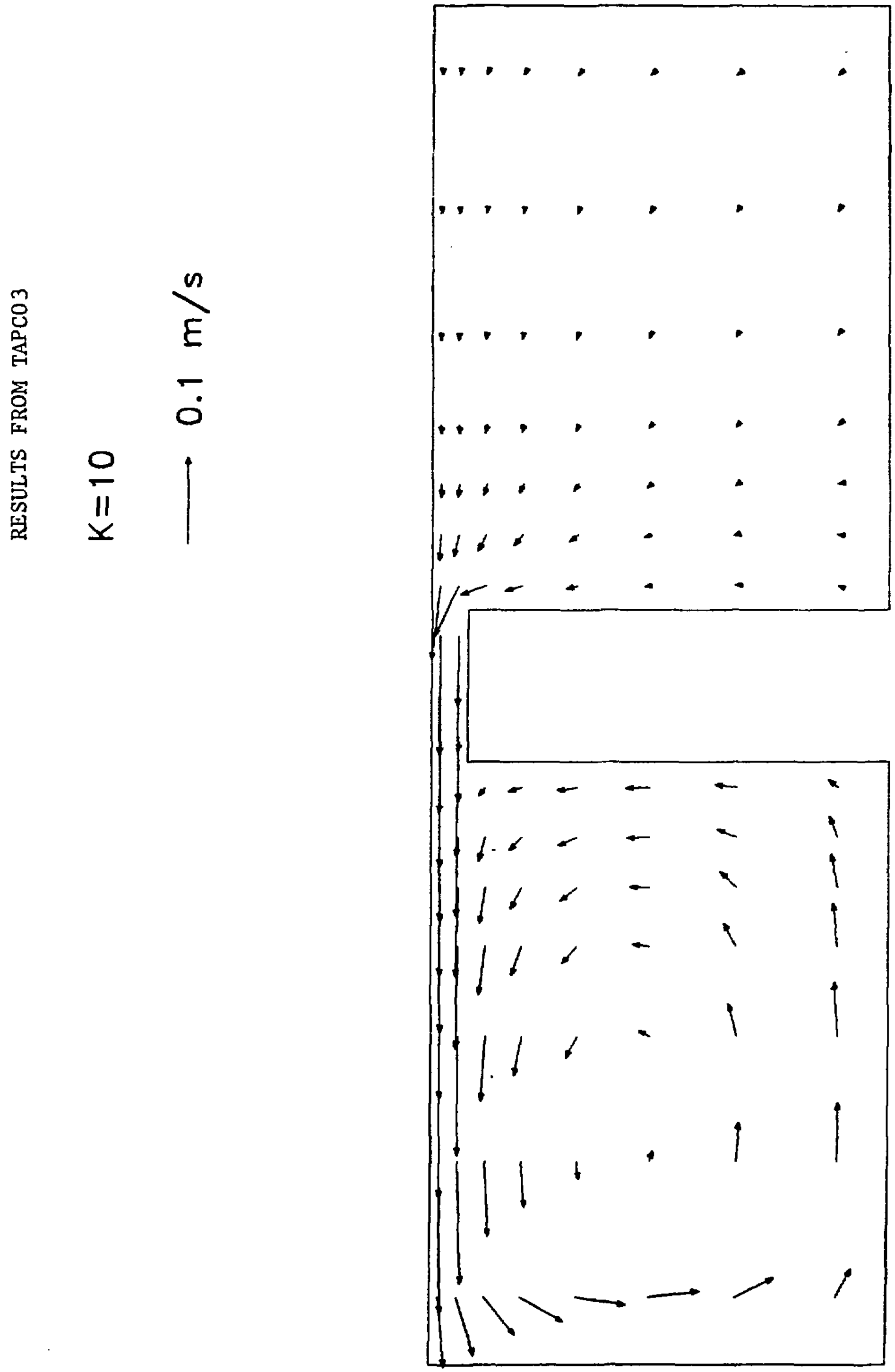

Figure 40

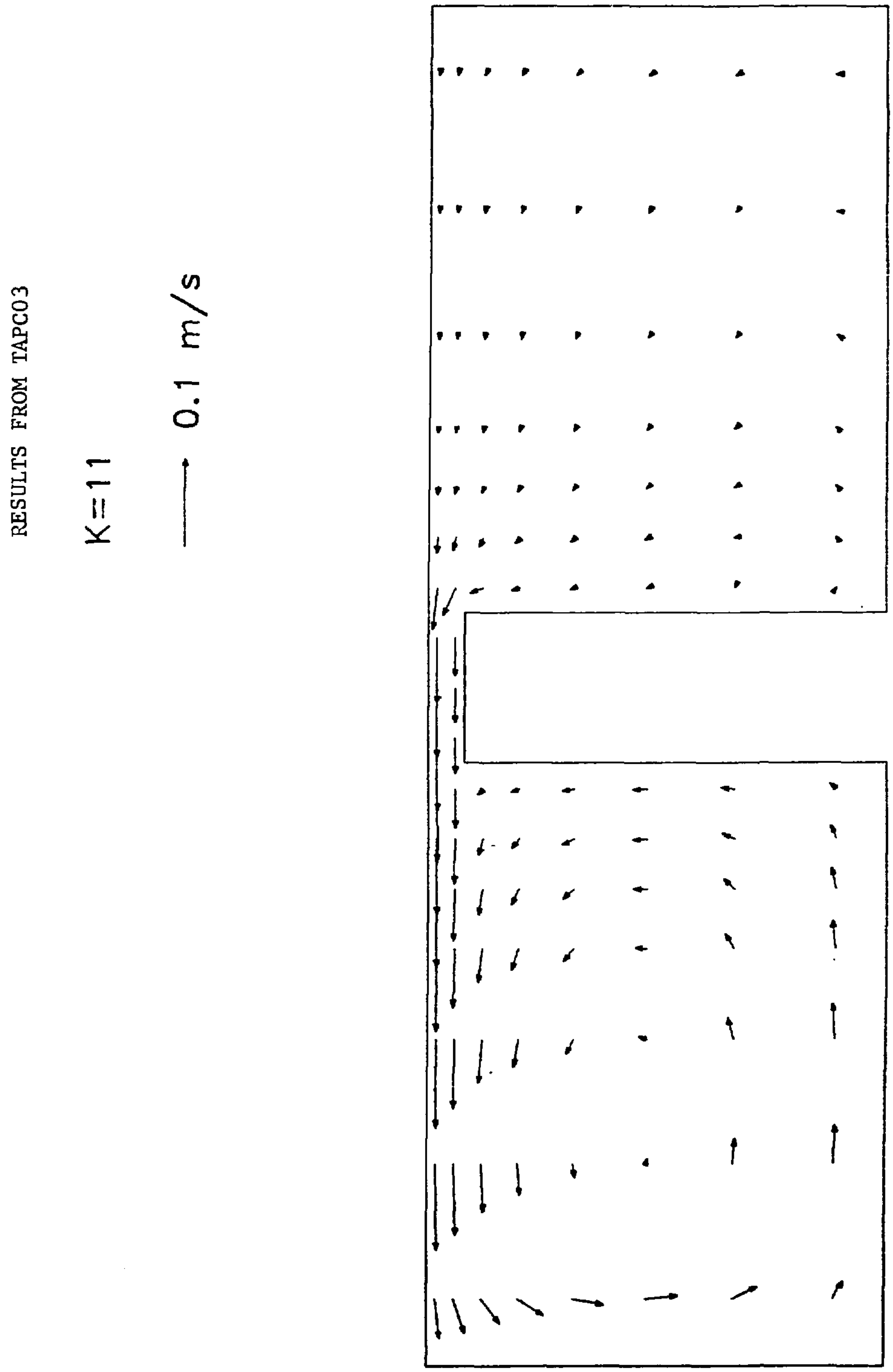

Figure 41

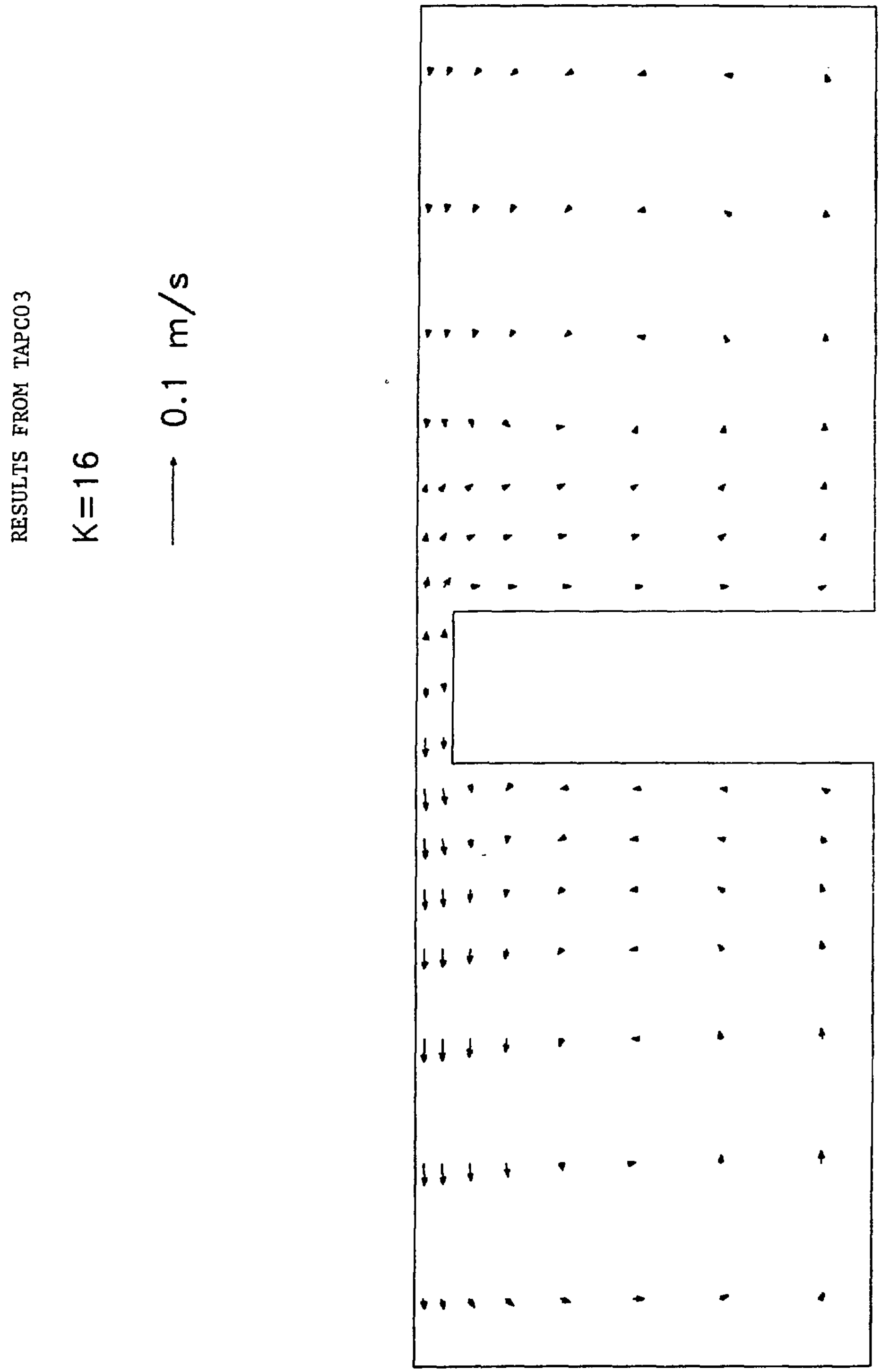

Figure 42

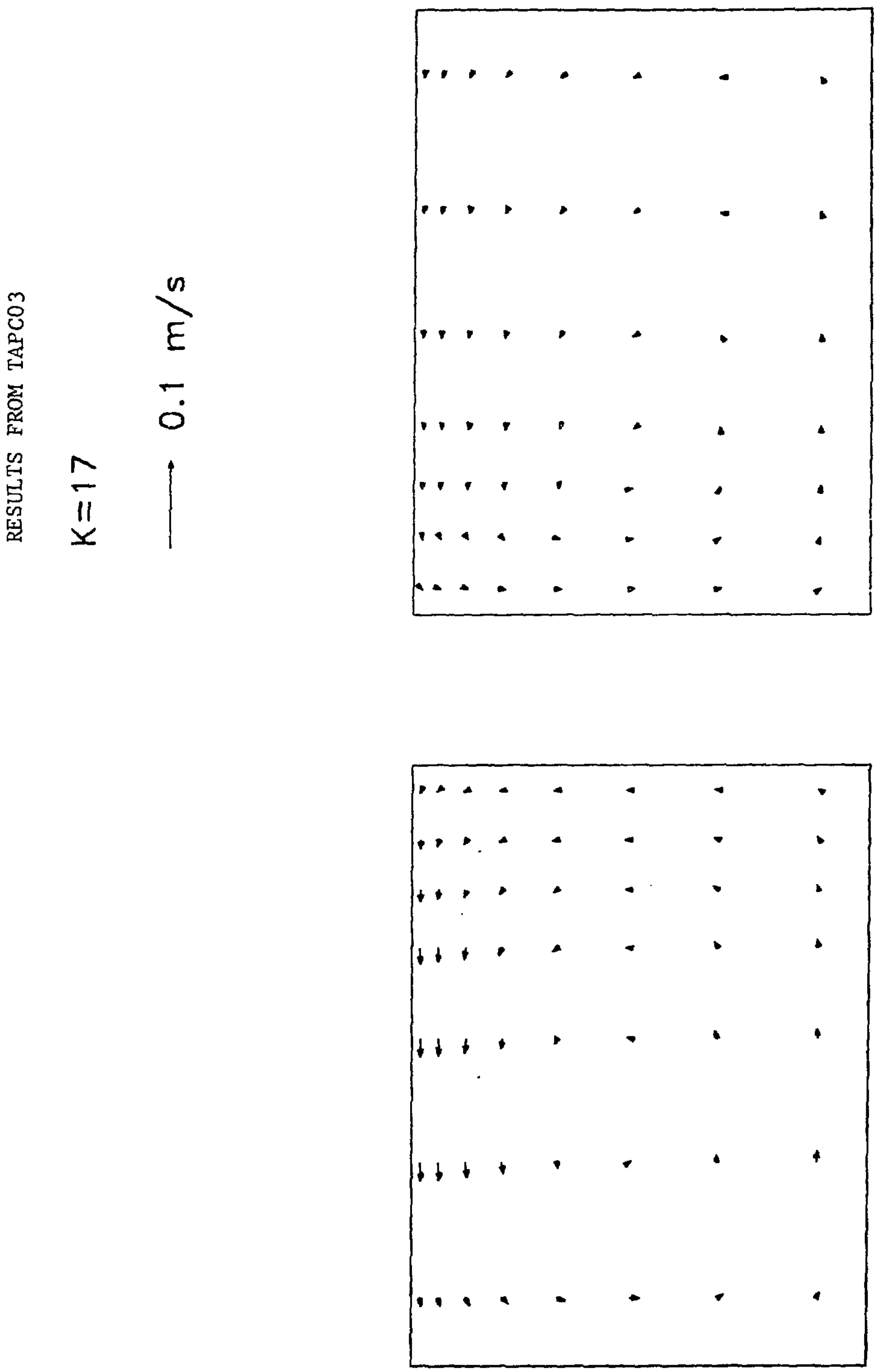

APPENDIX A

TABLE 1

COMPARISON OF DELTA PRESSURE ACROSS SLOT BETWEEN CHANNEL WALLS AND BETWEEN INLET AND OUTLET

CHANNEL HEIGHT	DELTA PRESSURE ACROSS SLOT		DIFFERENCE BETWEEN TWO DELTA PRESSURES
	CHANNEL WALLS	INLET OUTLET	
(METER)	(PASCAL)	(PASCAL)	(PASCAL)
0.310	156.46	145.36	11.10
0.359	111.98	112.34	-0.36
0.408	74.47	75.92	-1.45
0.457	55.94	56.62	-0.68
0.506	53.09	52.74	0.35
0.590	20.09	20.68	-0.59
0.710	15.50	15.33	0.17
0.830	12.38	12.16	0.22
0.950	8.31	8.19	0.12
1.030	11.72	10.95	0.77
1.070	13.47	12.71	0.76
1.110	20.12	19.06	1.06

TABLE 2 RESULTS FROM TAPC02

CHANNEL HEIGHT (METER)	CHANNEL PRESSURE DATA DONOR (PASCAL)	RECIPIENT (PASCAL)	DELTA (PASCAL)
0.052	1909.60	673.67	1235.93
0.156	1315.00	673.77	641.23
0.227	1051.60	673.83	377.77
0.266	920.98	673.87	247.11
0.310	818.09	672.73	145.36
0.359	817.94	705.60	112.34
0.408	806.38	730.46	75.92
0.457	786.46	729.84	56.62
0.506	763.87	711.13	52.74
0.590	682.17	661.49	20.68
0.710	574.59	559.26	15.33
0.830	464.37	452.21	12.16
0.950	353.34	345.15	8.19
1.030	282.82	271.87	10.95
1.070	247.98	235.27	12.71
1.110	214.98	195.92	19.06
1.150	192.26	150.48	41.78
1.190	149.19	121.22	27.97
1.230	141.68	90.81	50.87
1.360	-0.51	0.03	-0.54

TABLE 3 RESULTS FROM TAPC03

CHANNEL HEIGHT (METER)	CHANNEL PRESSURE DATA DONOR (PASCAL)	RECIPIENT (PASCAL)	DELTA (PASCAL)
0.052	89.83	-116.09	205.92
0.156	-14.41	-116.16	101.75
0.227	-65.03	-116.25	51.22
0.266	-91.45	-116.42	24.97
0.310	-102.88	-117.65	14.77
0.359	-86.66	-117.83	31.17
0.408	-53.11	-102.85	49.74
0.457	4.13	-56.18	60.31
0.506	71.52	12.73	58.78
0.590	95.26	92.54	2.72
0.710	114.58	112.55	2.03
0.830	102.71	101.50	1.21
0.950	80.14	79.80	0.34
1.030	63.79	62.73	1.06
1.070	54.42	54.33	0.09
1.110	44.17	45.43	-1.26
1.150	26.74	35.69	-8.95
1.190	15.92	29.16	-13.25
1.230	26.86	21.73	5.13
1.360	0.53	0.08	0.45

TABLE 4 RESULTS FROM TAPC02

CALCULATION OF INTEGRAL CROSS FLOW MASS TRANSFER

K	U(7) (M/S)	U(8) (M/S)	U-AVG (M/S)	DY(7)+DY(8) DZ(K) (M*M)	VOLUMETRIC FLOW RATE (M*M*M/S)	MASS FLOW RATE LOCAL (MEGAGRAM/HOUR)	MASS FLOW RATE INTEGRAL (MEGAGRAM/HOUR)	CHANNEL HEIGHT (METER)
5	0.1727	0.3186	0.2456	4.9784E-05	1.2229E-05	0.04390	0.04390	0.334
6	0.1873	0.3188	0.2530	4.9784E-05	1.2598E-05	0.04523	0.08913	0.383
7	0.1445	0.2488	0.1966	4.9784E-05	9.7900E-06	0.03515	0.12427	0.432
8	0.1161	0.1989	0.1575	4.9784E-05	7.8410E-06	0.02815	0.15242	0.481
9	0.1096	0.1849	0.1472	4.9784E-05	7.3307E-06	0.02632	0.17874	0.530
10	0.0556	0.0939	0.0748	1.2192E-04	9.1135E-06	0.03272	0.21145	0.650
11	0.0409	0.0681	0.0545	1.2192E-04	6.6446E-06	0.02385	0.23531	0.770
12	0.0331	0.0548	0.0439	1.2192E-04	5.3584E-06	0.01924	0.25454	0.890
13	0.0231	0.0382	0.0306	1.2192E-04	3.7368E-06	0.01341	0.26796	1.010
14	0.0279	0.0462	0.0370	4.0640E-05	1.5057E-06	0.00541	0.27337	1.050
15	0.0318	0.0529	0.0423	4.0640E-05	1.7211E-06	0.00618	0.27954	1.090
16	0.0544	0.0887	0.0715	4.0640E-05	2.9078E-06	0.01044	0.28998	1.130

TABLE 5 RESULTS FROM TAPC03

CALCULATION OF INTEGRAL CROSS FLOW MASS TRANSFER

K	U(7) (M/S)	U(8) (M/S)	U-AVG (M/S)	DY(7)+DY(8) DZ(K) (M*M)	VOLUMETRIC FLOW RATE (M*M*M/S)	MASS FLOW RATE LOCAL (MEGAGRAM/HOUR)	MASS FLOW RATE INTEGRAL (MEGAGRAM/HOUR)	CHANNEL HEIGHT (METER)
5	0.0167	0.0640	0.0403	4.9784E-05	2.0088E-06	0.00721	0.00721	0.334
6	0.1100	0.1659	0.1380	4.9784E-05	6.8677E-06	0.02465	0.03187	0.383
7	0.1559	0.2374	0.1966	4.9784E-05	9.7900E-06	0.03515	0.06701	0.432
8	0.1808	0.2845	0.2326	4.9784E-05	1.1582E-05	0.04158	0.10859	0.481
9	0.1865	0.2990	0.2427	4.9784E-05	1.2085E-05	0.04338	0.15197	0.530
10	0.0614	0.1261	0.0938	1.2192E-04	1.1430E-05	0.04103	0.19301	0.650
11	0.0348	0.0695	0.0522	1.2192E-04	6.3581E-06	0.02283	0.21583	0.770
12	0.0236	0.0436	0.0336	1.2192E-04	4.0965E-06	0.01471	0.23054	0.890
13	0.0132	0.0244	0.0188	1.2192E-04	2.2921E-06	0.00823	0.23877	1.010
14	0.0151	0.0251	0.0201	4.0640E-05	8.1686E-07	0.00293	0.24170	1.050
15	0.0136	0.0225	0.0181	4.0640E-05	7.3355E-07	0.00263	0.24433	1.090
16	0.0139	0.0210	0.0175	4.0640E-05	7.0917E-07	0.00255	0.24688	1.130

TABLE 6 RESULTS FOR TAPC02

CHANNEL HEIGHT (METER)	DONOR CHANNEL AREA AVERAGED VELOCITY (M/S)
0.104	1.559
0.208	1.559
0.247	1.560
0.285	1.560
0.334	1.464
0.383	1.390
0.432	1.331
0.481	1.284
0.530	1.240
0.650	1.187
0.770	1.148
0.890	1.116
1.010	1.093
1.050	1.083
1.090	1.072
1.130	1.059
1.170	1.059
1.210	1.059
1.250	1.059

TABLE 7 RESULTS FROM TAPC02

VELOCITY RATIO TRANSVERSE/DONOR	TRANSVERSE RESISTANCE COEFFICIENT	CHANNEL HEIGHT (METER)
0.1575	5.200	0.310
0.1728	3.507	0.359
0.1415	3.862	0.408
0.1183	4.523	0.457
0.1147	4.911	0.506
0.0603	7.211	0.590
0.0459	10.466	0.710
0.0383	12.854	0.830
0.0275	17.742	0.950
0.0339	17.124	1.030
0.0391	15.063	1.070
0.0667	7.882	1.110

```
**** GRID SUMMARY ****

IMAX=17  JMAX= 8  KMAX=20

 I= 1   X= 1.4300000D-03  DX= 2.8600000D-03
 I= 2   X= 4.2900000D-03  DX= 2.8600000D-03
 I= 3   X= 6.9100000D-03  DX= 2.3800000D-03
 I= 4   X= 8.8150000D-03  DX= 1.4300000D-03
 I= 5   X= 1.0058350D-02  DX= 1.0567000D-03
 I= 6   X= 1.1115050D-02  DX= 1.0567000D-03
 I= 7   X= 1.2171750D-02  DX= 1.0567000D-03
 I= 8   X= 1.3228450D-02  DX= 1.0567000D-03
 I= 9   X= 1.4285150D-02  DX= 1.0567000D-03
 I=10   X= 1.5341850D-02  DX= 1.0567000D-03
 I=11   X= 1.6398550D-02  DX= 1.0567000D-03
 I=12   X= 1.7455250D-02  DX= 1.0567000D-03
 I=13   X= 1.8511950D-02  DX= 1.0567000D-03
 I=14   X= 1.9755300D-02  DX= 1.4300000D-03
 I=15   X= 2.1660300D-02  DX= 2.3800000D-03
 I=16   X= 2.4280300D-02  DX= 2.8600000D-03
 I=17   X= 2.7140300D-02  DX= 2.8600000D-03
 J= 1   Y= 6.9850000D-04  DY= 1.3970000D-03
 J= 2   Y= 2.0955000D-03  DY= 1.3970000D-03
 J= 3   Y= 3.3020000D-03  DY= 1.0160000D-03
 J= 4   Y= 4.3180000D-03  DY= 1.0160000D-03
 J= 5   Y= 5.0800000D-03  DY= 5.0800000D-04
 J= 6   Y= 5.5880000D-03  DY= 5.0800000D-04
 J= 7   Y= 5.9690000D-03  DY= 2.5400000D-04
 J= 8   Y= 6.2230000D-03  DY= 2.5400000D-04
 K= 1   Z= 1.0204500D-01  DZ= 2.0409000D-01
 K= 2   Z= 2.5613500D-01  DZ= 1.0409000D-01
 K= 3   Z= 3.2738500D-01  DZ= 3.8410000D-02
 K= 4   Z= 3.6579500D-01  DZ= 3.8410000D-02
 K= 5   Z= 4.0950000D-01  DZ= 4.9000000D-02
 K= 6   Z= 4.5850000D-01  DZ= 4.9000000D-02
 K= 7   Z= 5.0750000D-01  DZ= 4.9000000D-02
 K= 8   Z= 5.5650000D-01  DZ= 4.9000000D-02
 K= 9   Z= 6.0550000D-01  DZ= 4.9000000D-02
 K=10   Z= 6.9000000D-01  DZ= 1.2000000D-01
 K=11   Z= 8.1000000D-01  DZ= 1.2000000D-01
 K=12   Z= 9.3000000D-01  DZ= 1.2000000D-01
 K=13   Z= 1.0500000D+00  DZ= 1.2000000D-01
 K=14   Z= 1.1300000D+00  DZ= 4.0000000D-02
 K=15   Z= 1.1700000D+00  DZ= 4.0000000D-02
 K=16   Z= 1.2100000D+00  DZ= 4.0000000D-02
 K=17   Z= 1.2500000D+00  DZ= 4.0000000D-02
 K=18   Z= 1.2900000D+00  DZ= 4.0000000D-02
 K=19   Z= 1.3300000D+00  DZ= 4.0000000D-02
 K=20   Z= 1.4600000D+00  DZ= 2.2000000D-01


 TOTAL NUMBER OF IRREGULAR CELLS                NM=    0
 TOTAL NUMBER OF CELLS                          NM1=2312
 TOTAL NUMBER OF IRREGUALR SURFACE ELEMENTS NL=    0
 TOTAL NUMBER OF SURFACE ELEMENTS               NL1=1460
```

```
 &SIZE
 NP1=2320
 NL1=1400
 NADJCC=0
 NMATRG=0
 NPAR=0
 NFORCE=1
 NSTREL=0
 NELPAR=0
 ITURKE=0
 IWIRE=0
 &END
 &GEOM
  IGEOM=0,
  IMAX=17, JMAX=8,  KMAX=20,
  NSURF=10, IFRES=1, LHPRNT=0,
  DX=2*0.00286, .00238, .00143, 9*.0018567,
     .00143, .00238, 2*0.00286,
  DY=2*.001397, 2*.001016, 2*.000508,2*0.000254,
  DZ=.20409, .10409, 2*.03841, 5*.049, 4*.12, 6*.08, .22,
  XNORML= 0, 0, 0, 0, 0, 0, 1, 0, -1, 0,
  YNORML= 0, 0, 0, 0, 0, -1, 0, 1, 0, 0,
  ZNORML= 1, 1, -1, -1, 1, 0, 0, 0, 0, -1,
  &END
REG -1.        11  17   1   8   1   1   1     D INLET
REG -1.         1   7   1   8   1   1   2     R INLET
REG -1.        11  17   1   8  20  20   3     D OUTLET
REG -1.         8  10   7   8  16  16   4     SLOT END
REG -1.         8  10   7   8   5   5   5     SLOT START
REG -1.         1   7   8   8   1   4   6     FLUID SURFACE
REG -1.        11  17   8   8   1   4   6     *
REG -1.         1  17   8   8   5  16   6     *
REG -1.         1   7   8   8  17  20   6     *
REG -1.        11  17   8   8  17  20   6     *
REG -1.         1   1   1   8   1  20   7     +X
REG -1.        11  11   1   6   1  20   7     *
REG -1.        11  11   7   8   1   4   7     *
REG -1.        11  11   7   8  17  20   7     *
REG -1.         1   7   1   1   1  20   8     +Y
REG -1.        11  17   1   1   1  20   8     *
REG -1.         8  10   7   7   5  16   8     *
REG -1.         7   7   1   6   1  20   9     -X
REG -1.         7   7   7   8   1   4   9     *
REG -1.         7   7   7   8  17  20   9     *
REG -1.        17  17   1   8   1  20   9     *
REG -1.         1   7   1   8  20  20  10     R OUTLET
END
 &DATA
  VELOC=1.559, 0.0, 8*0.0,
  KFLOW= 1, 1, -5, 2*3, -3, 3*3, -5,
  TEMP=10*20.0,
  ISTATE=0, IFENER=0,
  KTEMP=10*1,
  KTHCON=-1,
  IT=10,IFPROP=1,
       FCOH = 1.2750 E 6, FC1H =    5.35  E+3,
       FCORO= 9.9720 E 2, FC1RO=0.0
       FCOMU= 1.0100 E-3, FC1MU= 0.0
       FCOK = 8.00   E-1, FC1K =-   6.25  E-4,
  TURBV=.0055, NMATER=0,
 ISYMCH=1,  OMEGA=1.4,  IODCP=1,
 EPS1=1.E-4, EPS2=1.E-6, IDTIME=1,  RDTIME=0.9, DTENER=1.,
 IFITEN=0, EPS5=1.E-5, DDDHMX=0., OMEGAE=.15, ITMAXE=100,
 TEMPO=20.0, PRESO=101353., XPRESO=.004, YPRESO=.004,
 ZPRESO=1.460,
 GRAVZ=-9.8067, ITIBUG=0,  NTPRNT=-9999,  NTMAX=1,
 ISTPR=-1201,-1208,-2201,-2208,-3201,-3208,-9201,-9208,17208,
       8208,16208, 51003, 51010,
 NTHPR=-1201,-1208,-2201,-2208,-3201,-3208,-9201,-9208,17208,
       8208,16208, 51003, 51010,
 IFREB=1,   NREBRT=19,  IREBIT=20,  IZREB=0,
 NREBM=19*56,
 NREBZ=19*56,
 NFORCE=0,
 &END
```

```
  1  11  17   1   8   1   1     DON. CH. REB. CELLS
  2  11  17   1   8   2   2     DON. CH. REB. CELLS
  3  11  17   1   8   3   3     DON. CH. REB. CELLS
  4  11  17   1   8   4   4     DON. CH. REB. CELLS
  5  11  17   1   8   5   5     DON. CH. REB. CELLS
  6  11  17   1   8   6   6     DON. CH. REB. CELLS
  7  11  17   1   8   7   7     DON. CH. REB. CELLS
  8  11  17   1   8   8   8     DON. CH. REB. CELLS
  9  11  17   1   8   9   9     DON. CH. REB. CELLS
 10  11  17   1   8  10  10     DON. CH. REB. CELLS
 11  11  17   1   8  11  11     DON. CH. REB. CELLS
 12  11  17   1   8  12  12     DON. CH. REB. CELLS
 13  11  17   1   8  13  13     DON. CH. REB. CELLS
 14  11  17   1   8  14  14     DON. CH. REB. CELLS
 15  11  17   1   8  15  15     DON. CH. REB. CELLS
 16  11  17   1   8  16  16     DON. CH. REB. CELLS
 17  11  17   1   8  17  17     DON. CH. REB. CELLS
 18  11  17   1   8  18  18     DON. CH. REB. CELLS
 19  11  17   1   8  19  19     DON. CH. REB. CELLS
  1  11  17   1   8   1   1     DON. CH. REB. Z SURF.
  2  11  17   1   8   2   2     DON. CH. REB. Z SURF.
  3  11  17   1   8   3   3     DON. CH. REB. Z SURF.
  4  11  17   1   8   4   4     DON. CH. REB. Z SURF.
  5  11  17   1   8   5   5     DON. CH. REB. Z SURF.
  6  11  17   1   8   6   6     DON. CH. REB. Z SURF.
  7  11  17   1   8   7   7     DON. CH. REB. Z SURF.
  8  11  17   1   8   8   8     DON. CH. REB. Z SURF.
  9  11  17   1   8   9   9     DON. CH. REB. Z SURF.
 10  11  17   1   8  10  10     DON. CH. REB. Z SURF.
 11  11  17   1   8  11  11     DON. CH. REB. Z SURF.
 12  11  17   1   8  12  12     DON. CH. REB. Z SURF.
 13  11  17   1   8  13  13     DON. CH. REB. Z SURF.
 14  11  17   1   8  14  14     DON. CH. REB. Z SURF.
 15  11  17   1   8  15  15     DON. CH. REB. Z SURF.
 16  11  17   1   8  16  16     DON. CH. REB. Z SURF.
 17  11  17   1   8  17  17     DON. CH. REB. Z SURF.
 18  11  17   1   8  18  18     DON. CH. REB. Z SURF.
 19  11  17   1   8  19  19     DON. CH. REB. Z SURF.
END
HL  16559        11  17   1   8   1  20     DON. VELOCITY
END
=============  END OF DATA ===================
  TAPC02 DATA     JUL 27, 1981
```